2016

Studies of the Properties of Designed Nanoparticles Using Atomic Force Microscopy

Steve Matthew Deese
Louisiana State University and Agricultural and Mechanical College

STUDIES OF THE PROPERTIES OF DESIGNED NANOPARTICLES USING ATOMIC FORCE MICROSCOPY

A Dissertation

Submitted to the Graduate Faculty of the
Louisiana State University and
Agricultural and Mechanical College
in partial fulfillment of the
requirements for the degree of
Doctor of Philosophy

in

The Department of Chemistry

by
Steve Matthew Deese
B.S., George Mason University, 2012
May 2017

ACKNOWLEDGMENTS

I'd like to extend my sincere gratitude to all that have helped me along the way in my journey to obtain my Ph.D. in Chemistry. In particular, I'd like to thank my wife, my best friend, Rachel Deese. Her dedication, reliability, and exuberance for life have made my life an absolute dream.

I'm grateful to my mother, Jane Deese, for raising me and providing me with all the love and support to achieve whatever I set out to do.

My appreciation goes out to Bill Kane for every ounce of love and support he has provided me along the way. His steadfastness in raising me will never be forgotten and will always be remembered in the best of light.

My great friend and future business partner, Derek Stapleton, has stuck with me through life's ups and downs. I will be forever grateful and indebted to his friendship.

TABLE OF CONTENTS

LIST OF FIGURES

LIST OF ABBREVIATIONS

AFM – Atomic Force Microscopy

AM – Amplitude Modulation

CPD – Contact Potential Difference

EFM – Electrostatic Force Microscopy

FM – Frequency Modulation

FMM – Force Modulation Microscopy

HOPG – Highly Oriented Pyrolytic Graphite

KPFM – Kelvin Probe Force Microscopy

SPM – Scanning Probe Microscopy

TEM – Transmission Electron Microscopy

UHV – Ultra High Vacuum

ABSTRACT

The purpose of the research in this dissertation was to elucidate the intrinsic properties of how nanoparticles are different from bulk materials. This was done by mechanical and electronic studies of the properties of designed nanoparticles using advanced modes of atomic force microscopy. Information relating to the work functions, contact potential difference, Young's Moduli, elasticity, and viscoelasticity can be investigated using state-of-the-art atomic force microscope (AFM) experiments.

Subsurface imaging of polystyrene encapsulated cobalt nanoparticles was achieved for the first time using Force Modulation Microscopy (FMM) in conjunction with contact mode AFM. Previously prepared sample of polystyrene coated cobalt nanoparticles were studied. Tapping-mode AFM was used to evaluate the size of coated nanoparticles. Force modulation microscopy was used to visualize details of the outer polystyrene coating. Differences between the softer polystyrene outer coating and the harder cobalt nanoparticle core was visualized based upon the elastic and viscoelastic properties. Variances in sample elasticity were monitored via the amplitude channel that monitors the oscillation amplitude of the cantilever while scanning. Viscoelastic differences were mapped by the phase channel which provides information of the phase lag of the probe.

The identification of designed nanoparticles based upon electrochemical properties was evaluated using the Kelvin Probe Force Microscopy (KPFM) mode of AFM. The contact potential difference between the tip and the sample is measured using an AC bias that is offset with a compensating DC bias while operating in either tapping-mode or non-contact mode AFM. The contact potential difference is more commonly referred to as the difference in work function

between the tip and the sample. The work function of a material can be calculated using a reference material with a known work function. Cobalt nanoparticles and gold nanoparticles were imaged using KPFM and baseline experimental contact potential difference values were obtained. Thus far, co-deposition of a mixed nanoparticle solution led to inconclusive results as the experimental and theoretical contact potential difference values were calculated. However, future studies relating to this experiment are planned.

CHAPTER 1. INTRODUCTION

Approaches developed in this dissertation consist of discriminating between similarly sized nanoparticles through studies of the physical properties of selected nanoparticles. Applications of Force Modulation Microscopy (FMM) include elucidation of copolymer packing at the nanoscale, nanoparticle characterization, and quantitative elastic and viscoelastic measurements. Applications of Kelvin Probe Force Microscopy (KPFM) include fundamental nanoscale work function measurements, insight into nanoscale p-n junctions, and local density of states investigations. Fundamental research at the nanoscale with visualization of nanoparticle domains based upon changes in the elastic and viscoelastic properties can furnish molecular-level insight into the surface properties of nanomaterials. Experiments using advanced modes of AFM coupled with tapping-mode or contact mode AFM were designed for nanoscale studies.

1.1 Scanning probe microscopy at the nanoscale

The field of molecular and atomic-scale surface imaging emerged when the scanning probe microscope was introduced in 1981 with Binnig and Rohrer credited as the first to successfully experiment with the instrument.[1] Images with atomic resolution have been useful in furthering the fields of materials science, surface science,[2,3] polymer chemistry,[4] and molecular devices.[5] With invention of the original scanning probe microscope, more than 50 different imaging modes have been developed with more being developed as the technology improves. Newer modes couple topographical information with electronic, magnetic, and spectral properties of nanomaterials. Advancement of new modes continually increases resolution and contrast into the atomic realm. Description of the history of scanning probe microscopy as well

as operating principles of modes used in research will be presented in Chapter 2 of this dissertation.

1.2 Electrostatic force measurements of nanoparticles

Surface potential and estimates of the dielectric constant can be worked out through the imaging of samples with electrostatic force microscopy (EFM) and Kelvin Probe Force Microscopy (KPFM), as presented in Chapter 3. Together these modes can be used to produce detailed surface potential maps and material work functions for fundamental understanding of nanoscale surface science. In this study, nanoparticles of both cobalt and cerium oxide were deposited onto a substrate and image with AFM. The types of nanoparticles cannot be distinguished using conventional tapping-mode or contact mode techniques. Studies with EFM and KPFM were used to investigate differences in the electrostatic forces of the nanoparticles. The mode of EFM couples conventional tapping-mode AFM with an added AC bias that is applied between the tip and sample surface. The bias produces an oscillation of electrostatic forces that cause the probe to respond in different ways relative to the strength of the forces. Studies with KPFM build upon EFM by applying a backing DC bias to the sample to nullify the contact potential difference. When the work function of the tip is known, the work function of the sample can be calculated from the value given by the applied DC bias that nullifies the buildup of electrostatic charge between the tip and the sample.

1.3 Comparison of electrochemical properties utilizing the Kelvin Probe Force Microscope

A novel approach for differentiating between similarly sized nanoparticles was studied using the Kelvin Probe Force Microscope, as described in Chapter 3. In this study, cobalt nanoparticles and gold nanoparticles of similar sizes were imaged with KPFM, first, separately,

then as a co-deposited mixture on an HOPG substrate. One of the ways to distinguish between similarly sized nanoparticle species is to measure and compare the contact potential difference that is measured with the KPFM mode. Highly oriented pyrolytic graphite (HOPG) was used as a substrate to reduce the amount of surface contamination that has been shown to affect measurements of contact potential. There are promising new ways to try to distinguish between dissimilar nanoparticles using the Kelvin Probe Force Microscope.

1.4 Polymer-encapsulated metal nanoparticles studied with force modulation microscopy

Visualization of the hard and soft areas of nanoparticles was achieved through the use of Force Modulation Microscopy (FMM), as described in Chapter 4. In designed experiments, polystyrene-encapsulated cobalt nanoparticles were imaged with a home-built force modulation sample stage. Operated in contact mode, the piezoceramic chip in the stage vertically oscillates the sample at a programmed frequency. Nanoscale elastic and viscoelastic variances in the sample can be probed as the cantilever responds to changes, accordingly, through monitoring the amplitude and phase channels of the AFM. In theory, areas with a higher elasticity will absorb more of the energy of the cantilever causing the amplitude of the oscillation to be dampened. Conversely, harder areas, having a lower elasticity, will cause the tip to oscillate closer to the input driving amplitude of the piezoceramic. Viscoelastic variations are tracked through the phase channel as qualitative information about the time-dependence of sample deformation can be obtained. Quantitative information including the Young's modulus of the sample can be estimated when tip geometry is known. To prevent aggregation of the ferromagnetic nanoparticles, two-particle lithography was used for sample preparation.

1.5 Synopsis

Scanning probe studies of nanoparticles with experiments to evaluate the inherent properties of nanomaterials offers new ways of analyzing materials at the nanoscale. Details that may not be visualized simply through topographic channels can be studied with advanced measurement modes of AFM.

CHAPTER 2. EXPERIMENTAL APPROACHES WITH ATOMIC FORCE MICROSCOPY

2.1 Contact Mode

Contact mode atomic force microscopy (AFM) was first demonstrated in 1986 by IBM scientist Gerd Binnig with the first experiment conducted along with Calvin Quate and Christoph Gerber. In contact mode, a cantilever with a very sharp silicon nitride tip is raster scanned across a surface to deduce topographical sample information as well as complex tip-sample interactions. As the AFM probe is scanned across the surface, a diode laser is reflected off the back of the cantilever to a position sensitive photodiode. Sample topography is monitored by mapping changes in the laser height as read by the photodiode. Any vertical displacement of the laser caused by a change in flexing of the cantilever results in the servo correcting the position of the AFM probe so as to maintain the original scanning parameters.

There are three main channels of information that can be collected with contact mode AFM: topography, deflection, and lateral force or friction (Figure 2.1). A topographical image is generated by placing the cantilever in contact with the sample surface and applying a desired force. The contact force is commonly measured in volts and then converted to nanometers. Height variances are measured as the voltage needed to restore the cantilever to the original setpoint is tracked. The force that is applied is proportional to the spring constant of the cantilever and causes the cantilever to bend. The bending of the cantilever is kept constant during imaging in contact mode since the degree of bending is proportional to the applied force. The applied force is monitored by a position sensitive photodiode that captures the signal of diode laser reflected from the back of the cantilever. A +y axis displacement of the laser to the diode indicates an increase in force felt by the cantilever; i.e. a decrease in tip-sample displacement.

Signal generated by the photodiode is sent to the computer and the servo renormalizes the force applied to the cantilever to the original setpoint.

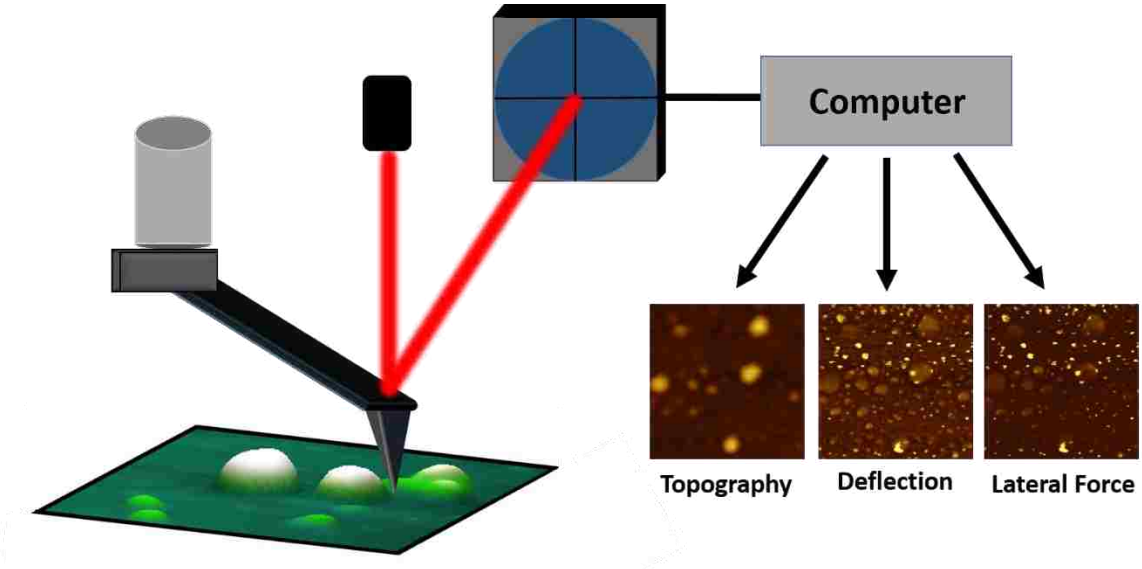

Figure 2.1: Schematic representation of contact mode atomic force microscopy

The deflection channel of information is essentially an error signal. It is the difference between the initial value for the setpoint of the cantilever and the return signal. This channel will yield no information of the sample properties, because the setpoint is chosen to remain constant.

Lateral force, and friction in some instances, is calculated from the torsional twisting of the cantilever caused by interactions between the sample and tip that occur while the tip is raster scanned across the surface. The tip-sample interactions can be both physical and electrostatic. The degree of torsional twisting of the cantilever is dependent upon tip-sample interaction as well as the how much the cantilever responds to strain.

In typical contact mode imaging, the force on the tip in the repulsive regime is on the order of 1×10^{-9} N and is kept constant by a computer controlled feedback loop. Commonly referred to as the simplest imaging mode of AFM, typical contact mode probes have spring

constants on the order of 0.05-5.0 N/m. A typical size of the tip apex is on the order of 10 nm. Sample imaging is usually limited to robust, non-biological samples that cannot be altered or destroyed by the imaging process. In the case of biological samples and samples that need more care taken while imaging, tapping-mode AFM is typically the preferred choice as it minimizes problems caused friction, adhesion, and electrostatic forces.

The use of integral and proportional gains while imaging in contact mode can limit the amount of error and help fine-tune other imaging parameters. This is accomplished with the use of a PID controller, short for proportional-integral-derivative controller, and an effective device used to minimize error over time. Accounting for present error values, the proportional gain controls output that is dependent on the current error values. However, error can build up over time causing the *P* gain to not sufficiently minimize the error signal. The Integral gain, I gain, takes past values of error into account in determining the necessary output to apply to the piezoelectric controller. The feedback control loop is not complete without the use of the PID controller. Adjustment of the integral and proportional gains, along with a few other parameters, controls the frequency of the feedback loop.

2.2 Tapping-mode Atomic Force Microscopy

Tapping-mode AFM, sometimes referred to as intermittent contact AFM, is a technique used to acquire high-resolution nanoscale images of a sample surface without damaging fragile samples (Figure 2.2). With tapping-mode, a cantilever with a very fine tip is mechanically actuated by a piezoceramic material at its resonant frequency causing the tip to vibrate in an undulating fashion. As with contact mode AFM, a diode laser is directed at the back of the cantilever and reflected to a four-quadrant photodiode. Any change in the displacement

amplitude of the laser to the diode reveals detailed information about changes in surface topography. Any lateral displacement of the laser is due to torsional twisting of the cantilever which details tip-sample interactions based on physical and electrostatic interactions.

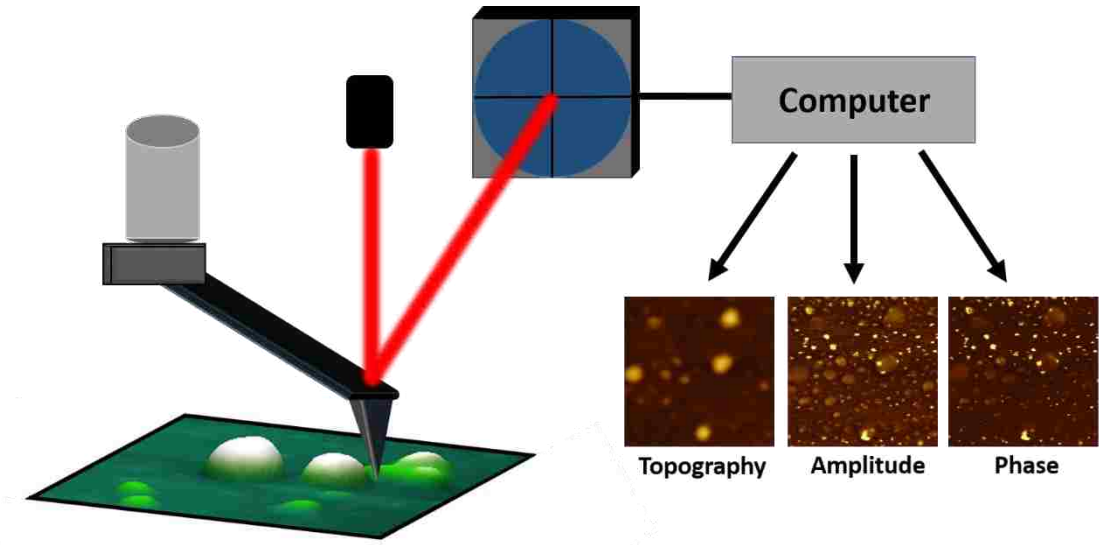

Figure 2.2: Tapping-mode atomic force microscopy

Once the diode laser light is intercepted by the photodiode, the signal is sent to the detector where a feedback loop is set to maintain a constant tapping amplitude of the cantilever. Attenuation or amplification of the tapping amplitude causes an electronic servo to renormalize the tapping height by making minor adjustments to the AC bias feeding the piezoceramic. The feedback loop enables the tip-sample distance to remain constant at a selected amplitude setting during imaging. A frequency sweep is performed to determine the resonance frequency of the cantilever. The tip must be an appropriate distance away from the sample as any interaction with the sample during the response sweep can dampen the desired tapping amplitude of the cantilever. Once the desired free amplitude of oscillation is chosen, the imaging amplitude will

be a specific percentage of the free amplitude depending on the amount of force that is needed for feedback to achieve good topographic resolution.

Tapping-mode produces three main output channels: topography, amplitude, and phase. The topography of the surface is collected from the vertical displacement of the laser into the photodiode. The phase channel details tip-sample interactions that cause the tip to be slightly altered from the tapping frequency. The phase lag is a difference in phase between the input driving signal and the return signal. Phase images have been used to map surface properties that include surface adhesion, viscoelasticity, and friction.

The intermittent force that is applied by the probe to the sample should be kept to a minimum as to not induce damage to the oscillator. Typical spring constants for tapping-mode AFM tips are in the range of 1-100 N/m which is greater than probes used in contact mode imaging. The advantages for using tapping-mode versus contact mode are associated with the reduction in adhesion, friction, and electrostatic forces. Forces that are typically present when the probe is in contact with a sample surface can damage the tip leading to imaging artifacts that are generally not encountered when imaging with tapping-mode.

2.3 Lord Kelvin and parallel capacitive metal plates

In 1898, Scottish physicist, Sir William Thompson, demonstrated that a potential energy difference is created between two parallel conductors when brought into electrical contact. The build-up of the potential energy was caused by the equilibration of the work functions between the metal plates. The work function is the amount of force that is needed to remove an electron from the surface of a conducting material to the vacuum energy level, an arbitrarily distant length. When two metals or semiconductors with dissimilar work functions are brought into

electrical contact with each other, electrons from the material with the lower work function flow to the material with the higher work function until the Fermi levels are aligned and equilibrium is reached. The Fermi level, in this specific case, is not a tangible energy level and is defined as the level at which there is a 50% probability of electron occupation. In essence, the parallel plates act as a capacitor and can store energy between the plates as a function of voltage, distance, and surface area. The contact potential is mitigated through an applied backing potential so that the surface charges disappear. The backing potential at which there is no residual build up in charge between the capacitor is equal and opposite in sign to the contact potential difference. Furthermore, the work function of a metal or semiconductor can be determined through normalizing the measurement to known work functions of different materials. As well, information about the distribution of local surface charges can be obtained for insulating materials.

2.4 Electrostatic Force Microscopy Theory and Previous Studies

The electrostatic force microscope (EFM) is an analog mode of AFM that adds an AC bias to modulate electrostatic forces between the probe and sample. Similar to tapping-mode or non-contact mode AFM, EFM is used to measure the topography of a surface while simultaneously acquiring local electrostatic forces as a function of position. The EFM is a powerful tool in nanochemistry research as nanoscale resolution for topography and surface potential images can be achieved. Typical applications of EFM include characterization of surface electrical properties,[6-8] interfacial charge transport measurements,[9] defect analysis of integrated circuits,[10, 11] and investigation of electronic properties of nanomaterials.[12, 13]

Since the introduction of scanning force microscopy, and more particularly Kelvin Probe Force Microscopy in 1991, the use of EFM for sample investigation and characterization did not become as popular until the 2000's. The increase in popularity corresponded to an increase in image resolution and the true potential of the instrument was realized as the technology advanced.[14] The original paper that details the ability for an AFM user to image electrostatic forces details the requirements that must be met for actual surface potential measurements. The first operational electrostatic force microscope was introduced by Nonnenmacher *et al*. with the invention of the Kelvin Probe Force Microscope (KPFM).[14] In some cases, increase in resolution can be attributed to ultrahigh vacuum coupled with cryogenic temperatures.[15, 16] Contact potential difference images of Au adsorbed onto Si(111) operating was achieved at the atomic scale in the noncontact regime by Kitamura *et al*.[17] Surface charge density and the investigation of domain structures in ferroelectric materials was reported by Hong *et Al.*[18] The next section will describe contact potential difference. Chapter 3 includes topics of EFM instrument operation, the theory of Kelvin Probe Force Microscopy and instrumental operation and resolution limits.

2.5 Studies of contact potential differences

A contact potential difference (CPD) exists when two dissimilar materials are brought into close, intimate contact with each other affecting the total electrostatic field between the two materials. The CPD between the materials results from formation of a thermal and chemical equilibrium formed within the junction.[19]

In the simplest case, the free electrons in metals occupy different energy levels in the material with the Fermi Level (E_F) considered in this case to be the energy level at which there is a 50% probability of electron occupation at a given time.[20] Since the Fermi level is a probabilistic

entity, it does not have to be a real, tangible energy level.[21] The Fermi Level in this case is commonly referred to as the chemical potential. In metals and solid-state materials, the chemical potential at the surface is a periodic distribution of potential energy determined by the crystalline structure of the material. Charges can be localized to areas of a crystalline structure that produce an electric potential that extends beyond the immediate surface of the material. The average amount of energy needed to bring an electron from the surface of the material to an arbitrary distance beyond the material surface is considered to be the work function of a material. The difference between the Fermi level and the electrostatic potential that the electron needs to overcome is measured in eV. When two crystalline materials are electrically connected, the electrons will reach diffusive and thermal equilibrium causing the Fermi level of each material to align with one another. Alignment of the Fermi levels creates an electrostatic field that exists across the junction that separates the materials. The potential difference that is created between opposite ends of the junction is referred to as the contact potential difference (CPD). The electrons that diffused from the solid with a higher Fermi level to the one with the lower Fermi level create a net positive charge on the material with a lower work function while concurrently causing the material with a higher work function to become more negatively charged. The total amount of transferred charge resides on the surface of the materials and creates an electrostatic potential difference, denoted V_{CPD}. By determining the CPD, the difference in work functions of the two dissimilar materials can be elucidated when standardized with a reference material.[20]

CHAPTER 3. ELECTROSTATIC FORCE MICROSCOPY AND KELVIN PROBE FORCE MICROSCOPY

3.1 Electrostatic Force Microscopy

Electrostatic properties of a surface can be intricately probed using electrostatic force microscopy.[22] Tip-sample interactions, and the effect on the cantilever oscillation are detailed by how the tip interacts with the sample when factoring in the presence of an electrical potential difference built up between the tip and sample. In simplest terms, the tip and the sample form a capacitor in which charge can be stored per unit of voltage.[23] The capacitance that is formed between the probe and the sample is dependent on the probe-sample separation and will invariably change with time. Electrostatic force microscopy was developed to map surface potential changes for a sample. Lift mode and variable bias are the two main modes used in EFM measurements and differ based on whether the tip deflection or the bias is monitored. In the this dissertation, a single-pass imaging technique was used with a triple lock-in amplifier system enabling simultaneous monitoring of topography and surface potential while maintaining feedback parameters at selected frequencies.

Lift mode operation is based upon the principle that the electrostatic forces generated between the probe and sample interact over a greater distance than van der Waals forces. Increasing probe-sample separation can separate electrical force information from topographical details. Probe-surface separation is typically in the range of 10-50 nm as this minimizes van der Waals forces while also continuing to be within range of electrostatic forces propagating from the surface.[24] Lift mode is a dual scan technique that generates a topographical map of the sample during the first scan and retraces the surface profile in the second scan as to maintain a

constant probe-sample separation.[25] Since the mechanical oscillation of the tip is null for the second scan, no feedback loop is required, enabling faster scanning.

The initial topography scan can be performed in either tapping-mode or contact mode. A constant voltage is maintained with the tip during the second pass as the probe retraces the topography map. An attractive electric field gradient will cause the tip to be pulled towards the sample whereas a repulsive gradient will cause the tip to be deflected away from the surface. The deflection of the cantilever, or change in frequency if using tapping-mode, is monitored in the second scan as it is proportional to the charge density of the surface.[26] Thereby, areas with a greater electrostatic potential caused by a bigger difference in work function between the tip and the sample will cause greater deflection of the cantilever.

The second mode of EFM, variable bias, generates surface potential images as the voltage on the tip is constantly adjusted to maintain constant deflection or amplitude of the cantilever. The absolute value of the electrostatic potential can be mapped out using the variable bias mode.

For EFM, tapping-mode or non-contact mode is coupled with an AC bias applied between the tip and the sample. Acquisition of detailed topographic maps of the sample surface is enabled while simultaneously providing high spatial resolution of surface potential. The AC bias is applied to modulate an electrostatic field between the probe and the sample. The total force felt by the cantilever is a combination of the electrostatic force from the applied AC bias, van der Waals interactions, and mechanical forces caused by oscillation of the cantilever above the sample.[27] The spatial resolution is dependent upon certain factors and will be addressed later. Amplitude modulation (AM) and frequency modulation (FM) are the two sub-modes in which EFM can be operated in while using tapping-mode. In amplitude modulation, the probe is oscillated above

the surface about 10% lower than the maximum amplitude of the mechanical resonance peak. The damping of the amplitude of the cantilever oscillation is monitored and held constant to acquire high resolution topography images. An AC bias is applied between the tip and the sample at a frequency generally between 5 kHz and 20 kHz making sure that the chosen frequency is not a factor of the mechanical resonance frequency of the tip. The frequency is chosen as to limit unwanted crosstalk between the mechanical oscillation of the tip and the applied AC bias frequency. The deflection, or amplitude, of the cantilever at $\omega_{elec.}$ is monitored by a second lock-in amplifier which interprets the electrostatic interactions between the tip and the sample. Further, additional force variations detailing a capacitive gradient can be observed at $2\omega_{elec}$.

3.2 Derivation of Forces Acting upon Cantilever

Further elucidation into the theory behind this technique is explained by deconstructing the system and treating it as a simple capacitor operated in tapping-mode. The conductive cantilever is mechanically oscillated near its resonance frequency, ω_0, at a distance of 10-50 nm from the sample surface. A potential difference is generated between the tip and the sample through a controlled bias voltage. The cantilever is used as a force detector that senses the electrostatic force created by alteration of the potential difference generated between the tip and sample. The total amount of force acting on the tip is comprised of van der Waals interactions, generated electrostatic forces, Coulombic forces, and mechanical force attributed to the oscillation of the tip.

According to theory, the tip will experience a force due to the capacitance gradient generated by a potential difference between the tip and sample. The electrostatic force experienced by the tip due to the capacitance gradient can be described as in Equation 3.1.

$$F_{(z,t)} = -\frac{1}{2}\frac{dC}{dZ}(V_S + V_{DC} + V_{AC}\cos\omega t)^2 \qquad \text{Eq. 3.1}$$

$$= -\frac{1}{2}\frac{dC}{dZ}\Delta V^2$$

$$= -\frac{1}{2}\frac{dC}{dZ}\left[(V_S(x,y) - V_{Probe})^2 + 2\big(V_S(x,y) - V_{probe}\big)V sin\omega t + \frac{V^2}{2}[1 - cos2\omega t]\right]$$

Where V_S is the potential of the sample, V_{DC} is the externally applied DC bias voltage, and V_{AC} is the set AC bias applied from the tip. The electrostatic force is proportional to the square of the voltage and the influence to the cantilever can be attributed to DC, ω, and 2ω contributions. The DC component is a static deflection of the cantilever attractively pulled towards the sample surface. The ω component is attributed to the varying AC electric field and the 2ω component is only dependent upon the capacitance between the electrodes caused by the AC bias. The ω component of force disappears when an offsetting DC bias is applied to the tip to nullify the contact potential difference such that $V_S + V_{DC} = 0$. The applied DC bias that compensates for the ω component of force is equal in magnitude but opposite in charge, therefore, quantitative contact potential difference measurements can be attained. For surface potential measurements, controlling the electrostatic force acting upon the tip is necessary for producing quantitatively accurate measurements.

3.3 Instrumentation design and operation for the electrostatic force microscope

The electrostatic force microscope (EFM) is an AFM with additional components that enable highly resolved measurements of the electric field gradient between the tip and sample

to be attained. Operating principles for EFM and KPFM can be better described with the help of Figure 3.1. Operation of EFM and KPFM for amplitude modulation topography imaging coupled with amplitude modulation electrostatic force imaging (AM-AM mode) while in intermittent contact mode is described. In AM-AM mode, a lock in amplifier (LIA1) is used to monitor the response of the oscillated cantilever being driven by the piezoactuator at its first mechanical resonance frequency. The second lock-in amplifier (LIA2) applies AC and DC biases to the probe and detects the electrostatic response of the cantilever from the photodetector. The AC bias frequency is specifically chosen as to not be a factor of the mechanical resonance frequency of the cantilever as a way to minimize crosstalk. The third lock-in amplifier (LIA3) is used to determine the amplitude response at $2\omega_{elec.}$ and is directly connected to the photodetector. In this case the amplitude detected is proportional to the electrostatic force thereby equivalent to dC/dZ. Local dielectric permittivity can be elucidated from the signal detected by the LIA3.[28, 29]

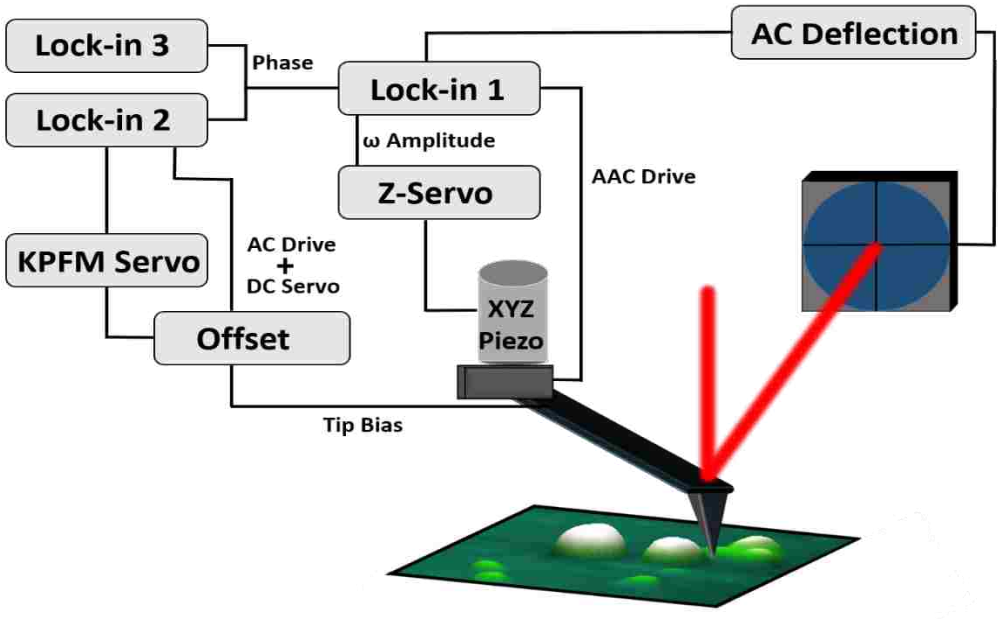

Figure 3.1 Instrument set-up for Electrostatic Force Microscopy and Kelvin Probe Force Microscopy. The AM-AM mode is depicted as FM-AM and has additional requirements.

The topography and surface potential of the sample are measured simultaneously and each require a feedback loop to generate high-resolution images. The first feedback loop is used to generate a topography image. The diode laser is reflected off the back of the cantilever to a photodiode detector. Operating in tapping-mode, the amplitude of the cantilever is fixed to a specific tapping amplitude setpoint determined by the user. The Z-servo sends a DC bias to the XYZ piezo to compensate for the detected change in tapping amplitude as monitored by lock-in amplifier 1. As such, a damping of the tapping amplitude is indicative of a decrease in the desired tip-sample separation and the tip is retracted from the sample, accordingly.

The feedback loop for the surface potential measurement works on the operating principle of minimizing the electrostatic forces generated by an oscillating AC bias between the tip and sample. Lock-in amplifier 2 is used to monitor the oscillation amplitude at the electrical frequency generated by the applied AC bias. A backing potential is used to minimize, or even nullify, the response of the tip at the electrical frequency. The magnitude of the backing potential that nullifies the signal at $\omega_{elec.}$ is output as the surface potential of the sample.

3.4 Kelvin Probe Force Microscopy

The working principle behind the Kelvin Probe Force Microscope is based upon the electrostatic buildup of charge between a sample and an oscillating tip. There is an inherent difference in work function between a platinum coated tip and a conducting sample. The work function is the energy difference between the Fermi level of the material and the theoretical vacuum energy level. Contact potential difference is used to refer to the difference between the work functions of the tip and the sample. When a reference material is used, the absolute work

function of a material can be found. This potential difference between the tip and the sample is commonly defined by Equation 3.2.

$$V_{CPD} = \frac{\varphi_{tip} - \varphi_{sample}}{-e} \quad \text{Eq. 3.2}$$

The ϕ_{tip} and ϕ_{sample} denote the work function of the tip and the sample, respectively. The contact potential difference is the difference in work function between two metals per unit charge.[30] The buildup in charge between the tip and the sample after alignment of the Fermi levels leads to extra forces beyond those associated with the mechanical oscillation of the tip. When the additional forces are nullified with a backing potential, it is assumed that the contact potential difference is equal in magnitude and opposite in charge to the backing potential. Nullification of the extra forces that act on the tip can be monitored. First, the tracking of the change in amplitude from its normal oscillation amplitude and, secondly, through tracking the frequency shift caused by the buildup of charge creating the two different imaging modes of AM-KPFM and FM-KPFM, respectively. The two approaches do not generate quite the same data. A change in the oscillation amplitude will determine an absolute contact potential difference, whereas, tracking the change in frequency enables measurements of the gradient in the contact potential difference. Once the contact potential difference of the sample is measured, the work function of the sample can be determined when the data is normalized to the known work function of the tip. The theory behind how a contact potential difference is formed between dissimilar materials is outlined in Figure 3.2.

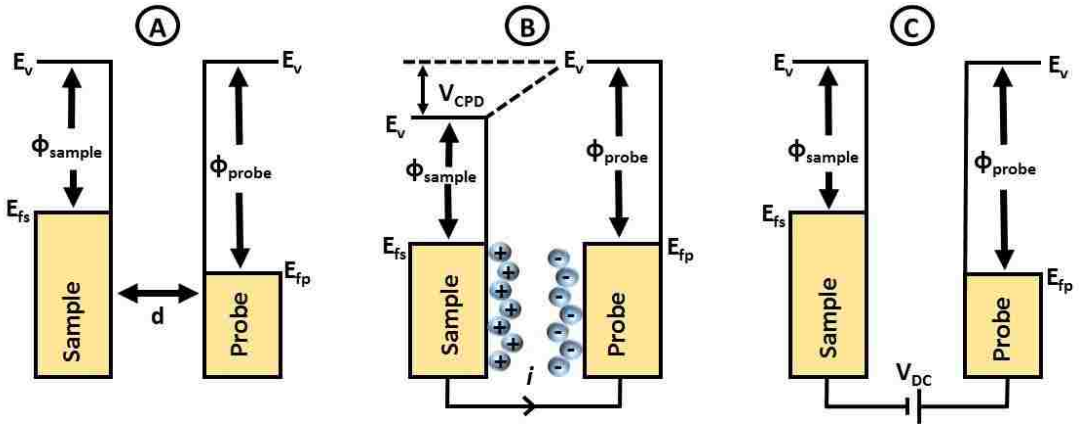

Figure 3.2 The electronic energy levels of the AFM probe and sample and how it evolves during KPFM imaging. (A) Probe and sample are not in electrical contact and are separated by distance, *d*. (B) Sample and probe are in electrical contact. (C) An externally applied bias (V_{DC}) is applied between the probe and sample to minimize the detectable contact potential difference.

An additional layer to the measurement of contact potential differences between the tip and sample arises when an AC bias plus a DC bias is applied to the AFM tip. The addition of the AC bias creates a time-dependent oscillation in the buildup of electrical forces in the capacitor that is then nullified with the backing DC bias. The force as a function of distance between the capacitive plates is determined by Equation 3.3.

$$F_{es}(z) = -\frac{1}{2}\Delta V^2 \frac{dC(z)}{dz} \qquad \text{Eq. 3.3}$$

In Equation 3.3, z is the distance between the probe and the sample perpendicular to the sample surface and ΔV is the difference between the contact potential difference and the voltage applied by the AFM. When a AC bias is applied to the tip, ΔV is summed up by the following Equation 3.4 with the bias being applied from the tip

$$\Delta V = (V_{tip} \pm V_{CPD}) + V_{AC}\sin(\omega t) \qquad \text{Eq. 3.4}$$

Equation 3.3 can be substituted into Equation 3.4 to form Equation 3.5 which is comprised of three separate parts detailing the forces that are present at each component.

$$F_{es}(z,t) = -\frac{1}{2}\frac{\partial C(z)}{\partial z}[(V_{DC} \pm V_{CPD}) + V_{ac}\sin(\omega t)]^2 \quad \text{Eq. 3.5}$$

The electrostatic force that arises from the DC bias contribution causes a static deflection of the cantilever where the magnitude of the force can be calculated as shown in Equation 3.6:

$$F_{DC=-}\frac{\partial C(z)}{\partial z}[\frac{1}{2}(V_{DC} \pm V_{CPD})^2] \quad \text{Eq. 3.6}$$

The contact potential difference between the sample and the tip is detected by minimizing the electrostatic forces that exist at the resonant tapping frequency.

$$F_{\omega} = \frac{\partial C(z)}{\partial z}(V_{DC} \pm V_{CPD})V_{AC}\sin(\omega t) \quad \text{Eq. 3.7}$$

The buildup of charge between the tip and the sample per unit voltage, the capacitance, can be monitored by measuring the additional forces that exist at 2ω. Capacitance microscopy can be performed based on Equation 3.8 and is not dependent upon the contact potential difference generated.

$$F_{2\omega} = \frac{\partial C(z)}{\partial z}\frac{1}{4}V_{AC}^2[\cos(2\omega t) - 1] \quad \text{Eq. 3.8}$$

The theory behind KPFM is dependent upon the additional electrostatic components that alter the resonant oscillation of the cantilever. In the case of single-pass KPFM, the cantilever is mechanically oscillated at close to the resonant frequency of the tip. An AC bias applied from the

tip to the sample causes additional electrostatic forces to arise which alter the amplitude of oscillation and the frequency of the cantilever's motion. Nullifying the additional forces with a compensating DC bias enables measurements of contact potential difference (CPD). Monitoring the additional forces at frequency ω caused by the AC bias is accomplished by using a lock-in amplifier. Because the output signal of the lock-in amplifier is proportional to the difference between the CPD and the applied DC bias, the CPD can be accurately determined as it is equal in magnitude and opposite in charge to the compensating DC bias. The value of the DC bias at every point in the scan is constructed into a two-dimensional potential energy map of the surface.

There are two different feedback loops that can be monitored to detect any deviation in tip oscillation caused by the buildup of electrical charges. The electrostatic forces built up at F_ω are experimentally determined through nullifying the amplitude at $\omega_{elec.}$, amplitude modulation, or by monitoring then negating the frequency shift at $\omega_{elec.}$, frequency modulation. In both modes, the topography of the sample is measured as it would be for tapping-mode or non-contact AFM. The additional feedback loop has no influence on the topographic measurements outside of possible crosstalk and is an adjunct mode to tapping-mode.

In amplitude modulation, the feedback signal is generated by monitoring the change in amplitude of the cantilever oscillation as caused by attractive and repulsive forces between the probe and sample.[31] Topography is measured at the first mechanical resonant frequency, ω, which is selected by the user after a frequency sweep of the cantilever is completed. To determine the resonance frequency of the cantilever, an AC bias is applied to the piezoceramic in the nosecone and a frequency sweep in the range of 1-300 kHz is performed. At resonance, the tapping amplitude of the cantilever will increase from the noise level to a greater value

depending upon the magnitude of the bias applied. The second resonant frequency can be monitored for any change in the oscillation amplitude of the mechanically actuated cantilever. However, changes in oscillation amplitude stemming from the addition of an AC bias occur at multiple frequencies and the second resonant frequency may not need to be monitored. In the case of the instrument used, frequencies on the order of 10-20 kHz were commonly used to acquire KPFM images in tapping-mode. Generally, a non-integer value for the monitored $\omega_{Elec.}$ is used as to limit the potential for crosstalk between the mechanical oscillation of the probe and the electrical field.

As AM-KPFM is operated in tapping- or non-contact modes of AFM, the tip-sample interaction decreases as the distance increases. As such, the oscillation amplitude of the cantilever should increase as the tip-sample distance increases. The tip-sample system can be analytically described by classical mechanics using the harmonic oscillator model as the force between the tip and the sample determines the change in amplitude.[32] The harmonic oscillator model dictates that the amplitude modulation mode of AFM measures the direct force between the tip and the sample and gives a single value, However, the force gradient between the tip and sample can be analyzed using the frequency modulation mode of KPFM.

Frequency modulation AFM provides insight into the force gradient between the probe and the sample as the shift in cantilever oscillation frequency is nonlinear and is dependent upon the tip-sample distance. It is assumed that the restoring force of the oscillating cantilever is large when compared to the interactive forces between the probe and sample so that the probe is only minimally perturbed. The FM-KPFM set-point is regulated by a feedback system that mitigates any shift in frequency back to the original set-point. The range of frequencies that can be used

for FM-KPFM is controlled by an upper and lower limit. The lower limit of detection is reached when cross talk between the topography signal and the AC bias occurs resulting in an oscillation in tip-sample distance at $\omega_{Mech.}$ Increasing the AC frequency lowers the degree of coupling between the topography and contact potential difference but frequency demodulator bandwidth limits the upper threshold. The fact that FM-KPFM determines the tip-sample force gradient rather than the absolute force value realized with AM-KPFM generally enables higher resolution with FM-KPFM.

3.5 Resolution and limitations of KPFM

The contact potential difference of a surface can be convoluted by factors such as tip geometry, localized capacitance, backing voltage, temperature fluctuations, and even atmospheric conditions. Tip geometry affects the capacitive buildup of charges between different points on the tip and the surface and the relative size of the tip in relation to minor areas of local electrostatic density.[33-35] The ideal tip-sample set-up for imaging using Kelvin Probe Force Microscopy is depicted in Figure 3.3. Ideally, the contact potential difference measurement occurs between just two points, the apex of the tip and the part of the sample directly underneath the tip when in contact with the sample.

The area of interaction between the probe and the sample can adversely impact the resolution of the surface potential measurement. For instance, a probe with a tip apex of 20 nm interacting with an area of the sample with a high charge density is localized to a nanometer sized domain. As the tip scans across the surface, electrostatic forces generated within the localized domain can interfere with the tip when not directly perpendicular to the domain resulting in convolution and will lead to inaccurate representations of the local surface potential. The

electrostatic forces have a range of up to several microns as opposed to van der Waals forces which generally fall between 10-20 nm.

Electrostatic forces that extend upwards of a few microns influence, not only the tip, but, the cantilever beam as well. This has been extensively modeled in previous literature and the electrostatic force acting upon the cantilever beam can be treated using a parallel plate capacitor model. Imaging of nanometer sized domains generate a total force acting on the tip/cantilever that is actually a weighted average of the forces between all points of the tip and cantilever. Since the cantilever is much larger than the tip, the increased interaction between it and the underlying substrate relative to the tip-substrate interaction results in lower lateral resolution; the color gradient and contrast of the image is not as sharp as it should be.

Further error deriving from sample convolution can be attributed to the feedback system that is used to minimize the electrostatic force contribution to the tip motion. Attempt at nullifying the electrostatic component of tip motion will include minimizing the contribution from the cantilever-surface capacitor system as well since the feedback system monitors the amplitude at $\omega_{elec.}$. A way to reduce or eliminate the convolution is to use a substrate with an equipotential surface that is much larger than the surface area of the cantilever. The weighted average at every position along the surface will be similar and divergence will stem from inhomogeneously altered areas of the prepared sample.

The detection mode for KPFM can also affect the resolution of imaging as force modulation KPFM has seemingly better resolution than amplitude modulation KPFM. An increase in resolution between FM-KPFM when compared to AM-KPFM can generally be attributed to the

fact that a force gradient is measured in frequency modulation mode whereas the total force is measured in amplitude modulation.

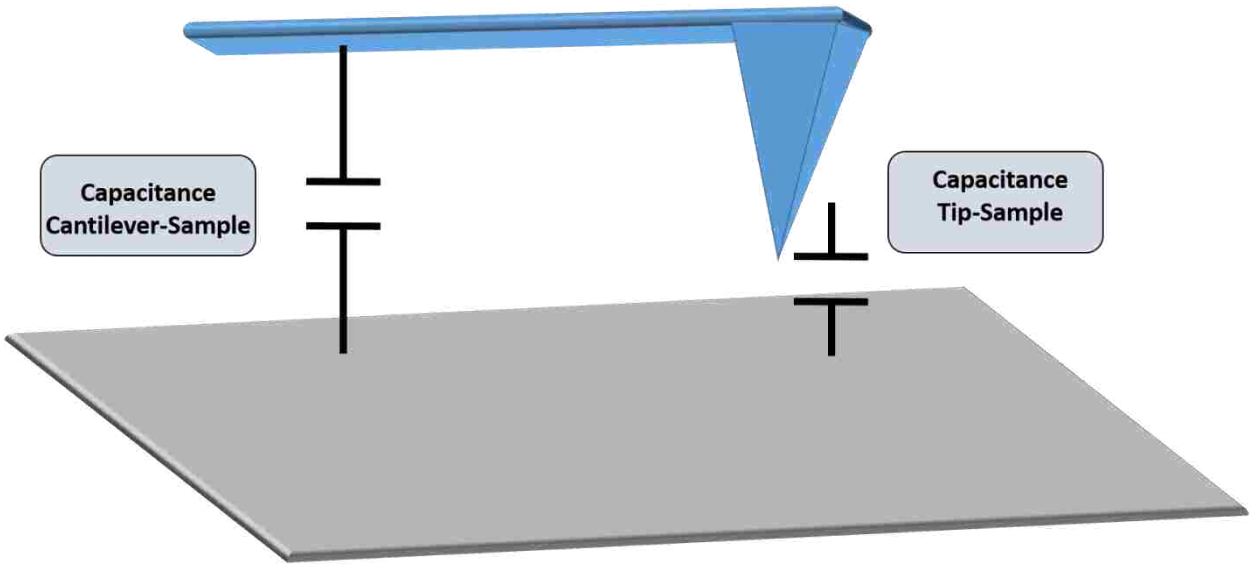

Figure 3.3 Multiple capacitive systems comprise the total capacitive gradient between the tip and surface.

Comparison between the two modes has been previously studied detailing that frequency modulation generally provides images with greater lateral resolution. In FM mode, the tip apex is mainly what is contributing to the measured signal whereas detection in AM mode is more dependent upon the shape of the entire tip.[36] However, AM mode is more widely used for KPFM because lower AC voltages can be used enabling the imaging of semiconducting materials that might have band bending when a greater bias is used.[37]

Ideally, the capacitance between the tip and the sample is measured in an atom-to-atom measurement. This is not theoretically possible as a capacitive gradient is built up between the tip and the sample and is dependent on the shape of the tip. The most common theoretical

models for mapping the tip-sample capacitive gradient relies on a cone-shaped probe with other models using a less accurate ellipsoid or sphere.[38, 39] Other models involve more in-depth calculations that will not be addressed here.[40] The cone-tip model is used in addition to the equations that the capacitance is derived from.

$$\Delta C_h = \varepsilon \frac{\Delta A}{d} \qquad \text{Eq. 3.9}$$

$$= \varepsilon \frac{2\pi h \tan(\theta)}{h+z} \Delta h$$

$$C_h = \int_0^h \frac{2\pi\varepsilon h \tan(\theta)}{h+z} dh \qquad \text{Eq. 3.10}$$

$$= 2\pi\varepsilon z \, tan(\theta)\left(\frac{h}{z} - ln\frac{h+z}{z}\right)$$

The capacitance in this model is derived from the shape of the cone probe and is dependent upon the width of the probe, probe height, and tip-probe distance.[41] The mode of capacitance detection is also integral to the resolution of the electrostatic measurement. Frequency modulation and amplitude modulation KPFM differ generally in one way; frequency modulation monitors the shift in resonant frequency of the tip caused by electrostatic forces whereas amplitude modulation depends on the change in tapping amplitude of the tip and is affected by the extra forces. The two modes of KPFM differ in how accurately the measurements can be used to detect the capacitance between the tip and the sample.

Frequency modulation KPFM is measured through monitoring of the frequency shift caused by a buildup in electrostatic forces accumulated between the tip and sample. Nullification

of these forces by a backing DC bias is a nonlinear process and it has been experimentally shown that half the signal can arise from only 0.3% of the conical probe.[42, 43]

Work function and capacitance detection through the use of amplitude modulation KPFM is achieved via monitoring the change in tapping amplitude of the tip at a frequency equal to the AC bias frequency that is applied the conical tip. In this case, an electrical AC bias is applied to the tip at a frequency much lower than the mechanical resonant frequency. Monitoring the change in the amplitude of the tip through this channel enables elucidation of qualitative electrostatic information about the sample. Nullification of the tapping amplitude at a specific frequency by using a backing DC bias quantifies the electrostatic measurements of work function and capacitance.

The resonance frequency bandwidth also affects imaging resolution. The Q-factor of an oscillating cantilever is a unit less quantity that is defined as the ratio of the height of the oscillation amplitude relative to the bandwidth at full width at half max. Resonators, such as the cantilever used for AFM imaging with higher Q-factors tend to resonate at greater oscillation amplitudes but have smaller bandwidths than ones with lower Q-factors. The ratio of frequency to the shift in frequency at full-width-half-maximum, the Q-factor of a typical tapping-mode cantilever is typically between 100-1000.[20, 32] Under optimal conditions of UHV and relatively low temperatures, the Q-factor can reach upwards of 50,000.[44] The resolution limit for KPFM is determined using Equation 3.11.

$$V_{CPD} = \frac{1}{\varepsilon_0 V_{AC}} \frac{d}{R} \frac{\sqrt{2k_B T k B}}{\pi^3 Q f_{res}} \qquad \text{Eq. 3.11}$$

The minimum sensitivity of KPFM measurements is determined by the smallest amount of force that can be detected in a given bandwidth which is also dependent upon the cantilever used for studies. Geometric and electronic factors make up the minimum detectable contact potential difference where V_{AC} is the applied bias, d is the tip-sample distance, R is the radius of the tip, k is the stiffness constant of the cantilever, Q is the Q factor, f_{res} is the resonance frequency of the cantilever, B is the bandwidth of detection, and k_B is Boltzmann's constant. Since operating parameters are a sizeable portion of the detection limit, maximization of the Q factor and minimization of the temperature are two keys to obtaining high resolution measurements. The Q factor can be optimized through use of a UHV system that rids the system of most contaminants that can dampen the amplitude or widen the bandwidth of the cantilever oscillation. The other variable that is based on instrument capability is the temperature as UHV systems also enable cryogenic temperatures to be used. Imaging under ambient conditions at a temperature below the freezing point of water causes the surface layer of water to freeze leading to damage to the probe. Imaging under UHV has been proven to increase imaging sensitivity by two orders of magnitude.[45, 46]

3.6 Operation and performance of Kelvin Probe Force Microscopy

The simplest way to measure the surface potential using Kelvin Probe Force Microscopy is to use a highly homogenous substrate to reduce the effects of convolution. Samples with highly homogenous surface charge density will require operation of the AFM in the electrostatic force microscopy mode as a null signal that s not needed for feedback. However, this is not always possible as surface potential measurements of nanometer-sized dimensions will be negatively

affected as the system diverges from the ideal theoretical capacitor design of two ideal electrodes.

The type of probe used is essential for electrostatic force microscopy measurements requiring specific coatings and spring constants.[47] In this dissertation, a platinum/iridium, n-doped silicon probe was the only probe that was used to analyze samples. Mechanical resonance frequency of the cantilever ranged between 45-115 kHz, lower than the usual resonance frequency of most tapping-mode tips. A force constant of 0.5-9.5 N/m is also lower for an EFM tip than one commonly used for tapping-mode. The chosen parameters enable the tip to be operated in intermittent contact mode or tapping-mode while providing optimal imaging parameters.

The tip is raster scanned across the surface at a fixed distance of 50-100 nm above the surface as to only interact with the sample through electrostatic forces. A non-contact feedback loop is used for the topography channel whereas the second lock-in amplifier detects electrostatic forces.

The electrostatic force detected by the tip-cantilever system is measured by applying both a DC bias and an AC bias to the tip whereby the AC bias varies with time ($V\sin\omega t$). The mechanical oscillation frequency, $\omega_{mech.}$, is chosen to be at or near the resonance frequency of the cantilever. Frequency of the AC bias, $\omega_{elec.}$, is chosen to be a non-integer value of the mechanical resonance frequency and is generally lower in frequency. The potential difference between the tip and sample caused by the AC bias produces an undulating electrostatic force with a frequency component of $\omega_{elec.}$. Controlling the DC bias applied to the tip as to minimize the electrostatically induced oscillation amplitude at $\omega_{elec.}$ enables surface potential mapping of the sample. Surface

potential measurements are performed by modifying the DC bias in incremental steps until the amplitude of the $\omega_{elec.}$ component is nullified. Typical imaging parameters include $\omega_{elec.}$ = 20 kHz, $\omega_{mech.}$ = 75 kHz with V_0= 8.5 V and are generally dependent upon each other. Separate optimization of individual components will not generate quality images; optimization of parameters must be done for the system as a whole.

3.7 Conclusion

The electrostatic force microscope and the Kelvin probe force microscope, have been shown to be an integral component in surface science and scanning probe microscopies. The two main operating modes, AM-KPFM and FM-KPFM, differ from one another in how the surface potential signal is tracked and measured. The AM-KPFM mode generates an absolute value for the potential and the FM-KPFM mode has a potential gradient. The surface potential, capacitive gradient, localized charge density, and electric dipole measurements can be monitored depending on the output channel making the instrument an integral tool for electrostatic force measurements.

CHAPTER 4. SUBSURFACE IMAGING OF THE CORES OF POLYMER ENCAPSULATED COBALT NANOPARTICLES USING FORCE MODULATION MICROSCOPY

Visualization of the hard and soft areas of a core-shell nanoparticle at the nanoscale has been achieved with the Force Modulation (FMM) mode of an Atomic Force Microscope (AFM). Polystyrene encapsulated cobalt nanoparticles were imaged and the differences between the soft outer polymer coating and the hard inner cobalt nanoparticle were resolved with high resolution. Using FMM, differences in the elastic and viscoelastic properties of the nanoparticles are visualized with nanoscale resolution by monitoring the return amplitude and phase signals as the AFM tip is scanned over areas of dissimilar elastic response. Areas of the sample with greater elasticity and viscoelasticity generate a weaker signal relative to harder areas because more of the energy associated with the cantilever oscillation is dissipated by the material. The nanoparticles were patterned using two-particle lithography to prevent aggregation to elucidate the diameters of the nanoparticles.

4.1 Background and introduction

The AFM is used in nanoscience to probe structures at the sub-micrometer scale with exquisite resolution.[1] Research using the AFM enables collection of data at the nanoscale that can quantify surface roughness, packing density, magnetic properties, as well as local density of states.[48-50] Quantification and characterization of ferroelectric and magnetic properties as well as detailing the polarizability and compressibility of nanoscopic materials has made the atomic force microscope a valuable tool.[51-53] Scaling down from the bulk into the nanoscale reveals differences in the mechanical properties and overall characteristics of materials. The Young's modulus, or modulus of elasticity, mathematically describes the degree to which a material can

be deformed elastically along a single axis. To measure the bulk modulus of a surface, measurements of the Young's modulus at each discrete point of the surface must be taken to construct a three-dimensional representation with the highest Young's moduli corresponding to the stiffest areas.[54, 55] The mode of FMM coupled with mapping enables elucidation of Young's modulus for nanomaterials.

Force Modulation Microscopy (FMM) is an advanced imaging mode of AFM that is coupled with contact-mode and is used in probing the surface elasticity and viscoelasticity at the nanoscale. Operated in contact mode, the tip is raster scanned across surface while the sample is concurrently modulated by a piezoelectric disk supplied with an AC current located in the sample stage. The tip experiences a small vertical oscillation along the z-axis as it scans as a result of the modulating sample stage. Changes in surface elasticity are measured by monitoring the change between the driving amplitude and return signal. Softer areas dampen the oscillation amplitude of the cantilever by a greater degree relative to harder areas. Furthermore, the phase signal details the viscoelastic properties of the surface as different areas will affect the phase of the tip modulation differently causing a phase lag in the return signal.[56] The complex changes in modulation amplitude, phase lag, and frequency shifts are disentangled by a computer algorithm enabling for nanoscale resolution of the elastic and viscoelastic surface properties.[57]

Previous studies using FMM detail the elastic and viscoelastic differences between block co-polymers, thin films, covalently-bound organic monolayers, and single crystals.[58-62] Characterization of block co-polymers at the nanoscale, for instance, gives insight into how a bulk material may behave since synthetic materials have a high dependence on how they are packed together at the molecular level. Additionally, subsurface imaging of nanoparticles within a

polymer film has been previously accomplished using Triple-Frequency AFM; a variant of the amplitude-modulation method.[63] In this study, the force modulation microscopy mode of scanning probe microscopy was used to characterize the variations in hard and soft regions of ferromagnetic polystyrene encapsulated cobalt nanoparticles. The nanoparticles were described previously in work by Bull *et al.* and TEM micrographs detailed the affinity to aggregate into long chains.[64] Other common nanoparticle characterization techniques like XRD, UV-Vis, XPS, and NMR are not able to visually and quantifiably differentiate between the different material domains of organic polymer encapsulated nanoparticles. Visualization of an outer polymer coating is only possible in TEM, under vacuum, and by staining techniques that incorporate metals into the polymer coating which may misrepresents the mechanical properties of the nanoparticles. Force modulation microscopy enables elucidation of the thickness of the polymer coating as well as the inner core nanoparticle.

Magnetic nanoparticles, particularly ones with organic or functionalized coatings, have been proposed as possible materials for hyperthermia treatments as well as visualization agents for use in MRI.[65] [66] The ability to control the dispersion and alignment of magnetic nanoparticles at a macroscale distance requires further research, as controlling their spread in the human body is vital for medical treatments. Furthermore, magnetic nanoparticles typically have finite size effects and surface effects that stem from the quantum confinement and the breaking of symmetry at the outer edge of the nanoparticle.[67] Catalytically active magnetic nanoparticles can be easily removed from a reaction and are ideal for lowering the costs attributed to separation of the nanoparticles from the desired product.

To image the nanoparticles with FMM, a designed sample stage was constructed which contains a piezoactuator in the middle of the stage directly beneath the sample. For sample evaluation, the AFM is operated in contact mode while the cantilever is raster scanned across the surface. An AC current supplied to the piezoelectric actuator causes the sample to vibrate at a desired frequency specifically chosen by the operator so that the frequency and magnitude of vibration is precisely controlled by the input AC signal. Changes in amplitude and phase depend on the driving frequency selected. The contrast of the constructed image is ultimately dependent upon the differences in mechanical properties of the material. The polystyrene outer coating has a greater elasticity and viscoelasticity than that of the cobalt core resulting in contrast changes for amplitude and phase channels. Thus, for this experiment, the subsurface features of polystyrene encapsulated cobalt nanoparticles were revealed through the use of FMM.

Elucidation of core-shell nanoparticles is useful for the future development of multicomponent nanoscale systems. Particle lithography was used to arrange and spatially segregate the nanoparticles along the surface to enable better evaluation of details by the AFM tip.[68] A mesosphere mask was first deposited onto the sample and dried under ambient conditions. This was followed by depositing a drop of a suspension of the nanoparticles onto the dried mesosphere mask.

4.2 Experimental Approach

The polystyrene encapsulated cobalt nanoparticles were received from Dr. Pyun's group at the University of Arizona. The nanoparticles were synthesized as previously reported.[64] Silicon wafers doped with boron of roughly 5 x 5 mm^2 dimension were obtained from Ted Pella Inc., Redford, California, and were used as the substrates. Substrates were cleaned in a Piranha

solution containing sulfuric acid (96% EMD Chemical Inc., Gibbstown, NJ) and hydrogen peroxide (30%, Sigma-Aldrich) at a ratio of 3:1 (v/v). Piranha is a strong oxidizing agent and must be handled with care. After 1.5 hours submerged in the solution, substrates were rinsed with deionized water (Milli-Q, Millipore, Bedford, MA) and dried with argon. Monodisperse silica mesospheres were purchased from Thermo Fisher Scientific, Waltham, Massachusetts. The silica mesospheres were washed three times with deionized water via centrifugation to remove any surfactants or charge stabilizers. Centrifuging the suspension for 15 min at 14000 rpm produces a pellet which was then resuspended in deionized water.

Particle lithography was used to prepare samples. A sample of 500 nm silica mesospheres was suspended in high purity deionized water. Next, 15 µL drop of the suspension was deposited onto the silica substrates and left to dry for 24 h under ambient conditions. The polymer encapsulated cobalt nanoparticles (0.5 mg/mL) were suspended in a solution of methylene chloride. A drop of 20 µL was deposited onto the previously prepared substrated with a mask of silica spheres. The sample was dried under ambient conditions for 24 h and then imaged with AFM.

A model 5500 scanning probe microscope (Agilent Technologies, Chandler, AZ) equipped with PicoView v1.12 software was used for AFM characterizations. The system was operated with an open-loop feedback for continuous scanning in contact mode. A homebuilt sample stage containing a piezoceramic actuator in the center was used to modulate the sample for FMM experiments. Data was acquired with Picoscan v5.3.3 software and the digital images were processed with Gwyddion (version 2.31) open source software supported by the Czech Metrology

Institute. [26] A nonmagnetic silicon nitride cantilever from Bruker with a spring constant of 0.01 N m^{-1} was used for tapping mode and FMM imaging (Veeco Probes, Santa Barbara, CA).

4.3 Results and Discussion

The polystyrene encapsulated cobalt nanoparticles were first characterized using tapping mode AFM. Clusters of cobalt nanoparticle deposited on a silicon substrate are shown in Figure 4.1. The uniformity in particle size and shape is revealed with a representative topography frame in Figure 4.1a.

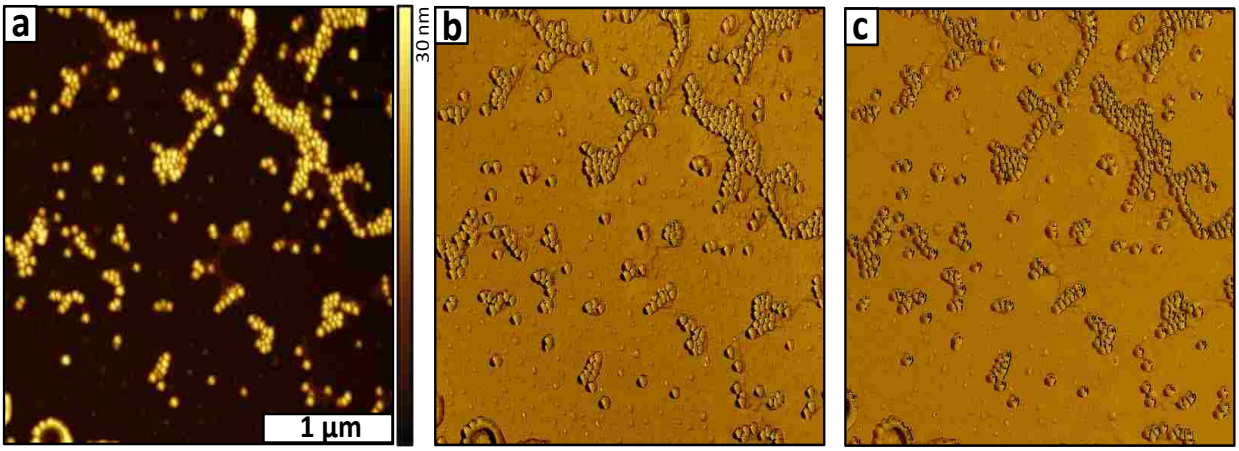

Figure 4.1 Polystyrene encapsulated cobalt nanoparticles imaged with tapping mode AFM; (a) topography, (b) trace phase, (c) re-trace phase.

The average size of the encapsulated cobalt nanoparticles is 25.0 nm ± 3.0 nm as acquired from 100 AFM height profiles. Nanoparticle sizes between 25-26 nm were most prevalent as revealed in Figure 4.2. Both the left and right scan of the phase images are shown due to the presence of a tip artifact in the left image. The clusters formed from drying deposited suspensions make it difficult for the AFM tip to penetrate the sample and obtain very fine sample details. The aggregation of nanoparticles can give misleading nanoparticle height measurements as the tip may not be able to fully penetrate between areas of clusters.

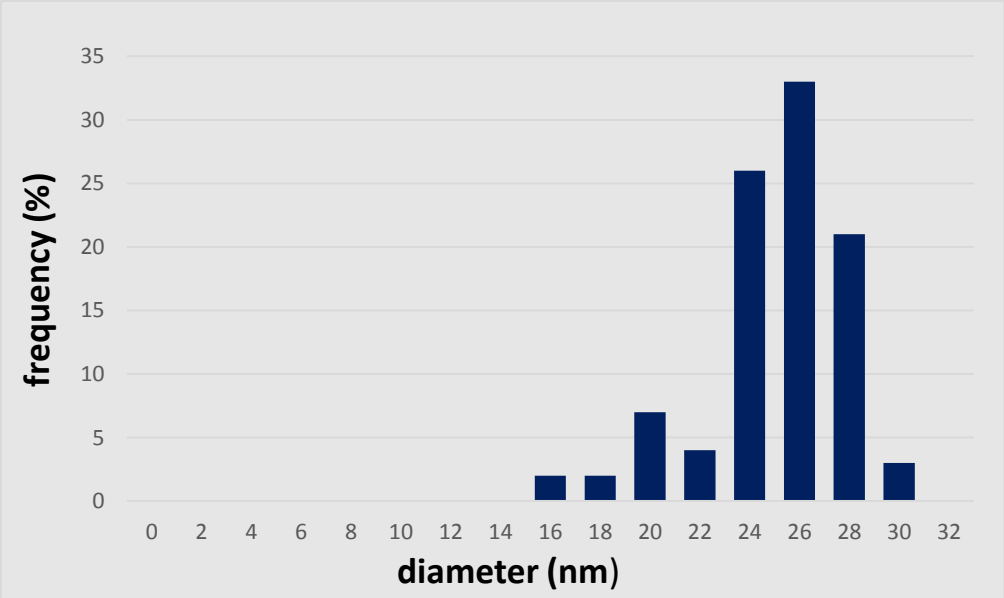

Figure 4.2 Size distribution of polystyrene encapsulated cobalt nanoparticles acquired from AFM height profiles (n=100).

To solve the problem of sample aggregation, the nanoparticles were patterned using particle lithography. For particle lithography, the solution of nanoparticles was added to a substrate with a latex mask. The mask was prepared by depositing a drop of mesospheres on the substrate which was then dried under ambient conditions. The mesospheres were subsequently removed according to a previous method.[69] The method of mesosphere removal was used to prevent disturbing the underlying rings of nanoparticles which can be washed away with solvents.

A sample prepared with particle lithography was imaged to visualize how the nanoparticles pack when organized by a surface mask of latex as viewed in Figure 4.2. Previously, the magnetic nanoparticles were shown to aggregate into long chains when imaged with TEM.[17] A partial ring comprised of the nanoparticles is visible in the lower left corner of Figure 4.2a. Although tapping mode images provide topographic details, there is no information of the subsurface characteristics of the encapsulated nanoparticles.

Nanopatterned rings of polystyrene encapsulated cobalt nanoparticles were imaged using FMM to visualize and map surface elasticity and subsurface structure as shown in Figure 4.3. The periodicity of the nanorings measured 500 nm as determined by the size of the latex mask. The AC current that was applied to the piezoceramic in the sample stage was deactivated midway through imaging to evaluate the FMM set-up. For the topography frame, the size of the nanoparticles remain the same between the top half of the image when the sample is being oscillated shown in Figure 4.3a compared to the bottom half of the image when the AFM is operating in contact mode. Furthermore, the topograph in Figure 3a is not affected when the sample modulation is interrupted. The amplitude and phase images reveal clearly the changes in experimental parameters when the field is applied or discontinued as seen in Figures 4.3b and 4.3c.

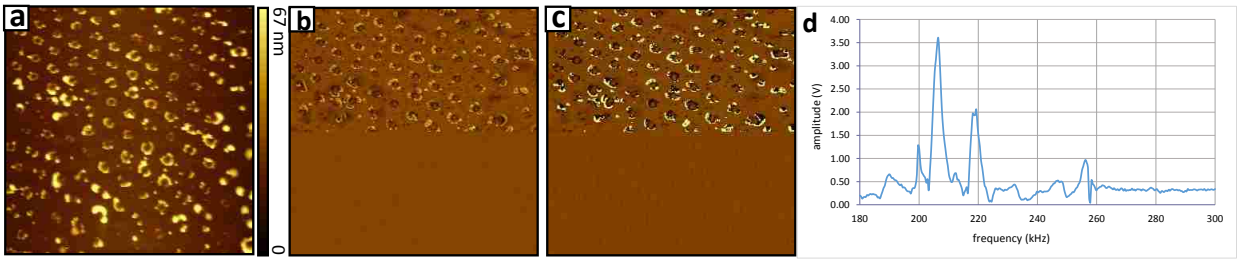

Figure 4.3 Ring nanopatterns of polymer encapsulated cobalt nanoparticles imaged with FMM. (a) Topography image acquired using FMM and concurrently acquired (b) amplitude and (c) phase images. (d) Frequency sweep used to determine various resonance frequencies.

The amplitude channel furnishes information about the elasticity of the sample as in the example of Figure 4.3b. Areas with lighter contrast reveal the size and shape of the cobalt core of the nanoparticles which is harder as compared to softer areas of the surface and outer polystyrene layer. When imaging in FMM, the elasticity of the sample is related to the change in the deflection of the cantilever as the AFM tip scans across the surface in contact with the

vibrating sample. Softer areas of the sample are compressed to a greater extent and thus absorb more of the energy of the oscillating cantilever which dampens the amplitude signal.

The phase shift between the driving signal and AC deflection signal is used to map the viscoelastic properties of the sample. The resolution and color contrast of images is determined by the selected feedback parameters and is based on the type of sample imaged as well as the resonance frequency selected for imaging. In this example, the phase channel ,Figure 4.3c, displays better resolved images than the amplitude frame, Figure 4.3d.

A resonance spectrum with the drive activated was obtained with the tip in contact with the sample as shown in Figure 4.3d. The AC drive was set to 5% and a frequency of 205 kHz was chosen for imaging parameters with FMM. Other resonance peaks including the ones at 200 kHz and 220 kHz were evaluated and showed morphology details in the amplitude and phase images, however 205 kHz provided the best details and contrast and therefore was chosen as the imaging frequency for FMM studies. Prominent peaks were not observed at frequencies below 180 kHz or above 300 kHz for this example.

The ring patterns of polymer encapsulated cobalt nanoparticles were imaged with FMM at a frequency of 205.7 kHz and 5% drive frequency seen in Figure 4.4. The topography images reveal details of the nanoparticle size, shape and arrangement as viewed in Figures 4.4a and 4.4d. A few individual nanoparticles are evident. The magnified view of the sample in Figure 4.4 discloses an area where nanoparticles were randomly distributed in between the rings and provides exquisite details of differences in the elastic response of the domains of the sample.

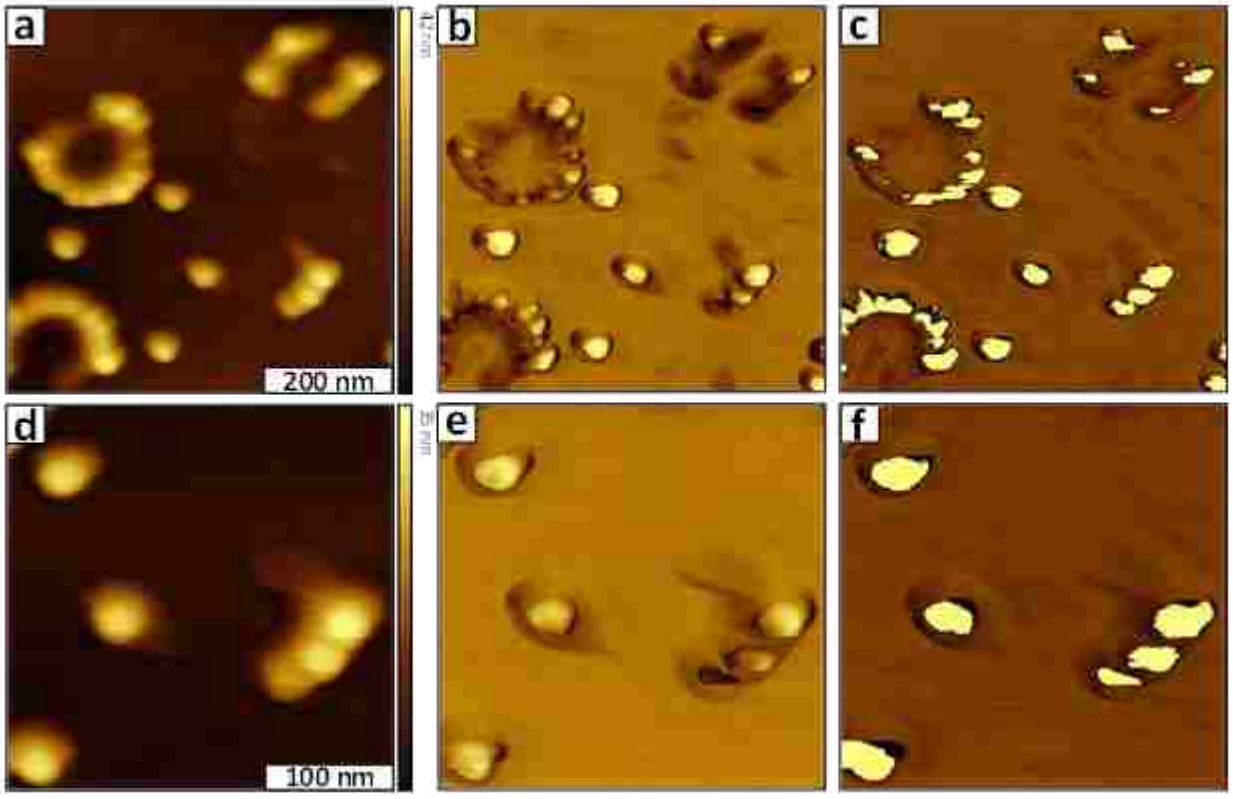

Figure 4.4. Metal cores of polymer encapsulated cobalt nanoparticles revealed with FMM to enable subsurface imaging. (a) Topography, (b) amplitude, and (c) phase images and subsequent enlarged views of six nanoparticles; (d) topography, (e) amplitude, and (f) phase frames.

For FMM, the amplitude images are constructed from tip-sample interactions in which softer areas of the sample absorb a greater amount of kinetic energy from the oscillating tip-sample causing the AC deflection signal to dampen with respect to the driving signal. A response in amplitude is attributable to the interaction between the tip and a hard surface as caused by a greater deflection in the oscillation of the cantilever. The changes in amplitude are displayed as differences in contrast. For this example the harder areas are brighter and softer areas are darker as shown in Figures 4.4b and 4.4e. There is a sharp change in contrast apparent between the brighter nanoparticle cores and the surrounding darker areas of polymer coating presented in Figures 4.4b, 4.4c, 4.4e, and 4.4f.

Information of surface viscoelasticity is provided in the phase images in Figures 4.4c and 4.4f. The phase shift is related to how the sample changes the resonance oscillation of the tip through the time it takes to reestablish its equilibrium position. For FMM experiments with encapsulated metal nanoparticles, not only information of surface morphology can be acquired, views of what is under the surface can be obtained with optimized parameters. Within the amplitude and phase frames, a surrounding shell of polymer provides a softer surface region that is mapped out surrounding the metal cores to demonstrate subsurface imaging.

A control experiment was done to acquire FMM images of polystyrene nanoparticles that do not contain a metal core (Figure 4.5). The frequency that was chosen for each experiment was obtained by taking a resonance sweep of the tip interacting with the sample and selecting the most prominent peak which was at the 205 kHz peak used previously. The same AFM cantilever was used in each experiment to minimize the differences in experimental parameters. A representative image from the control experiment shows a single polystyrene nanosphere ~45 nm in diameter within a 300 x 300 nm^2 area in Figures 4.5a-4.5c. A smaller, individual polystyrene encapsulated cobalt nanoparticle ~30 nm in diameter is shown in Figures 4.5d-4.5f within an area of 200 x 200 nm^2.

The topography frames obtained with FMM provide views of the nanoparticle spherical shapes, size and surface morphology (Figures 4.5a and 4.5d); the images are comparable to those acquired with contact mode. Amplitude and phase images are shown for the isolated polystyrene nanoparticle in Figures 4.5b and 4.5c respectively.

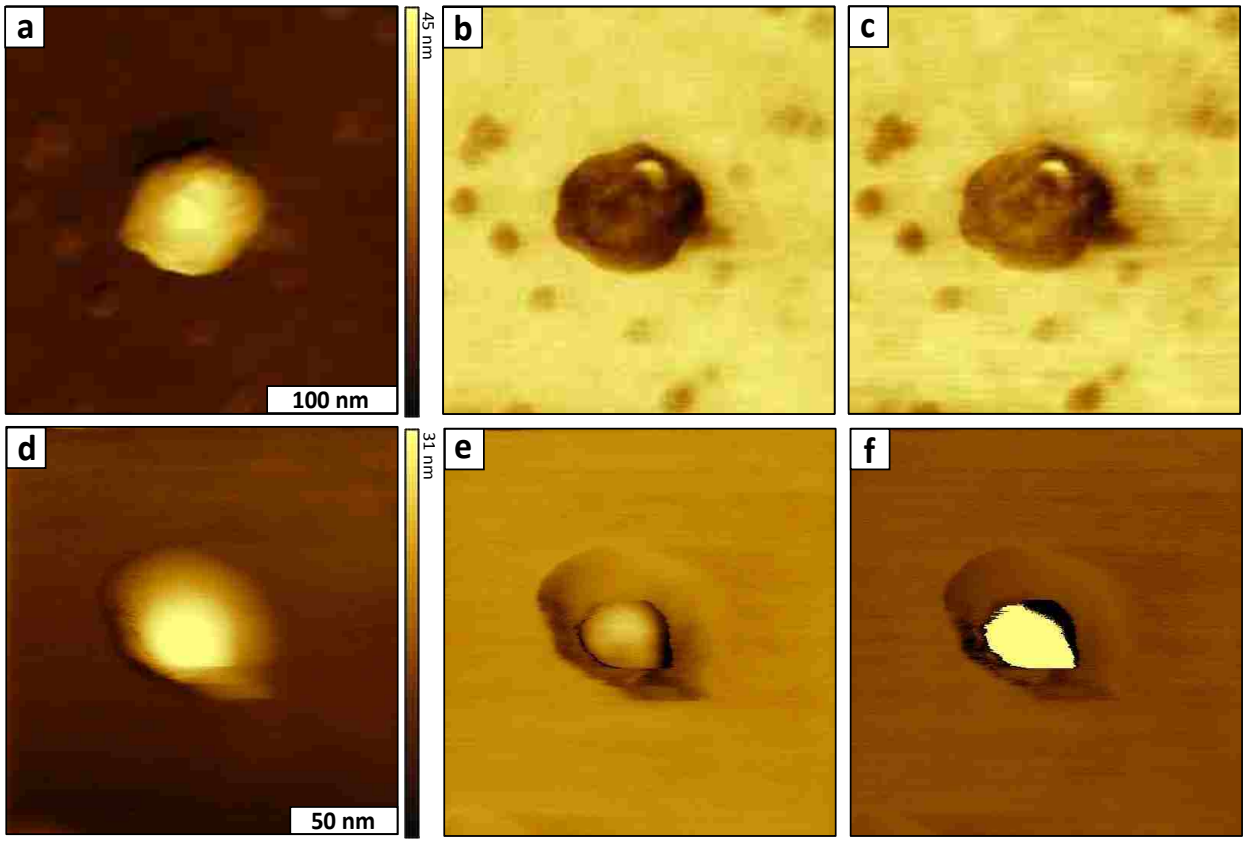

Figure 4.5. Comparison of a polystyrene nanoparticle versus a polystyrene encapsulated cobalt nanoparticle. Corresponding (a) topography, (b) amplitude, and (c) phase image of polystyrene nanoparticle. Encapsulated cobalt nanoparticle (d) topography, (e) amplitude, and (f) phase frames.

The frames reveal interesting details of the surface of the nanoparticle, with a circular region surrounding the nanoparticle. As the tip is scanned across the nanoparticle, the motion of the tip is influenced by the edges of the nanoparticle to respond differently. However, the bright region of a nanoparticle core is not evident in Figures 4.5b and 4.5c. The nanoparticle is comprised of a single elastic domain and has a higher elasticity and viscoelasticity than the silica surface. The amplitude and phase images of the polymer encapsulated cobalt nanoparticle (Figures 4.5e and 4.5f, respectively) reveal distinct differences in the elastic and viscoelastic

response of the probe to enable subsurface images of the inner cobalt core and surrounding polymer shell.

Force Modulation Microscopy images may be visually misleading. Images of the polystyrene encapsulated cobalt nanoparticles visually indicate that the polymer coating comprises 20-30 % of the nanoparticle thickness. Polymer coating thickness can be adequately approximated by comparing the average size of the cobalt nanoparticles, as determined by TEM, and contrasting that data with the average size measurements performed by AFM. With enough useable data points, the average polymer thickness can be approximated as simply the difference between the two averages. In this case, Pyun *et Al.* determined cobalt nanoparticle size to be 25 ± 3.9 nm whereas tapping-mode AFM measurements, which take the polymer coating into account, concluded that the particle size is 25 ± 3.0 nm. This high degree of overlap in the calculated size distributions leads to an inconclusive result in polymer coating thickness determination. However, it can be approximated that the polymer coating thickness is 0.1 – 2.0 nm as it is within the margin of error for this technique.

4.4 Conclusions

Force modulation microscopy was successfully used to accomplish subsurface imaging of polymer encapsulated cobalt nanoparticles with nanometer resolution. Although the nanoparticles are ferromagnetic and have a tendency to aggregate when dried on surfaces, we were able to apply particle lithography to control the arrangement of nanoparticles on the surface. A sample with a ring arrangement of nanoparticles was evaluated with FMM to reveal differences in elastic response for the polymer coating and inner metal core. The FMM mode of scanning probe microscopy has proven to be valuable in the characterization of polymers and

nanoparticles. In our studies, The FMM mode has enabled direct visualization between an outer organic layer and an inner metal core that is not possible with other characterizations. Future studies using FMM with nanoparticles will address analysis of the changes in thickness of polymer coatings as a function of reaction variables such as time, temperature, and concentration. The thickness of the outer organic coating of nanoparticles is important in determining the impact that polymers have on catalytic and other properties of encapsulated nanoparticles.

CHAPTER 5. CHARACTERIZATION OF DISSIMILAR NANOPARTICLES USING KELVIN PROBE FORCE MICROCOPY

Experiments to differentiate between different nanoparticles of similar size were designed using the Kelvin Probe Force Microscopy (KPFM), an advanced mode of the atomic force microscope (AFM).

5.1 Background and Introduction

High resolution imaging of the nanometer and molecular level has continually improved with the use of the atomic force microscope (AFM) which was originally introduced in 1986 by Gerd Binnig and Heinrich Rohrer.[1] Three-dimensional topographic images of surfaces at the nanometer scale have evolved by adding measurement capabilities to the instrument making it possible for surface properties of magnetism,[70-72] Young's modulus,[73, 74] elasticity,[75, 76] force,[77-79] and electrostatic potential to be evaluated.[27, 80, 81] The classical Kelvin probe technique was the inspiration for the successful design of the Kelvin Probe Force Microscope (KPFM) which was implemented to measure the work functions of materials at the nanoscale. Used in conjunction with noncontact- or intermittent-contact AFM, KPFM can be operated in both frequency and amplitude modulation mode.

The electrostatic potential between the tip and the sample can be analyzed both quantitatively and qualitatively using the imaging modes of electrostatic force microscopy (EFM) and Kelvin probe force microscopy (KPFM). Contact potential difference (CPD) measurements provide insight into oxide layer formation,[82, 83] adsorption layers,[84, 85] nanomaterial reactivity,[19] and dopant concentration levels in semiconducting materials.[86-88] There is an electrostatic potential, or contact potential difference, between two dissimilar metals that arises due to a

difference in work functions. Determination of the absolute quantity of the work function can be made through calibration of the probe with a material with a well-known work function. Another possible option is to compare different materials oriented on a surface with a well-known work function as is the case with highly oriented pyrolytic graphite (HOPG).

Multiple modes of KPFM, including amplitude modulation (AM) and frequency modulation (FM), are commonly used to characterize the contact potential difference between metals and semiconductors. However, the difference between the two modes is related to the surface potential data that is generated. Amplitude modulation uses a backing DC potential to offset the oscillating electrostatic field generated by the AC bias fed between the tip and the sample. Minimization of the detected oscillation amplitude at the applied AC bias frequency with the DC bias generates an integer value for the contact potential difference. Frequency modulation, however, generates a surface potential image that indicates the gradient of the contact potential difference between the tip and the sample. Amplitude modulation was used in this study as imaging in frequency modulation mode requires a much higher threshold for eliminating noise.

Accurate measurements of work function are challenging to attain as there are many factors that can alter the measurement or lead to inaccurate data such as the effects of oxide layer formation, adsorbates, and humidity.[89] Ideally, ultrahigh vacuum (UHV) and cryogenic temperatures are the optimal condition for which to operate the KPFM to lower the undesirable effects that naturally occur when imaging under ambient conditions.

In the experiments described in this Chapter, when the imaging parameters under ambient conditions are optimized, the contact potential difference can be adequately

determined by coupling the placement of an AC bias between the tip and sample and concurrently operating the instrument in tapping-mode. The work functions of cobalt nanoparticles along with gold nanoparticles were determined using the intermittent contact mode of the AFM coupled with the amplitude modulation approach for contact potential difference measurements. The nanoparticles were first characterized independent and electronic properties were measured to elucidate the associated surface potential. Experiments were designed to distinguish between the cobalt and gold nanoparticles based upon the inherent electrostatic properties and not on the size, morphology, or other attributes.

5.2 Materials and Methods

Gold nanoparticles were deposited onto an HOPG substrate and dried under reduced pressure at 50 C. The gold nanoparticles were first imaged with tapping-mode AFM and then with the KPFM servo turned on to ensure that crosstalk between the AC bias and the mechanical oscillation of the tip was minimized. The ferromagnetic cobalt nanoparticles that were used for studies were synthesized by the Pyun research group at the University of Arizona and were determined to have an average diameter of 24.6 ± 2.8 nm with some measured to be 40-50 nm in diameter. The cobalt nanoparticles were deposited onto a HOPG surface and left to dry under vacuum at 50 C.

A model 5500 scanning probe microscope (Agilent Technologies, Chandler, AZ) equipped with PicoView v1.12 software and with electrostatic force microscopy capabilities was used for AFM characterizations. The system was operated with an open-loop feedback for continuous scanning in contact mode. Data was acquired with Picoscan v5.3.3 software and the digital images were processed with Gwyddion (version 2.31) open source software supported by the

Czech Metrology Institute. A Pt/Ir-coated probe with a force constant of 0.5-9.5 N m^{-1} was used for contact mode, EFM, and KPFM. (Nanosensors, Switzerland)

5.3 Results and Discussion

Four channels of measurement acquired simultaneously for a single experiment are shown in Figure 5.1. The images are representative of multiple scans of a sample of gold nanoparticles prepared on HOPG. Details of the size and shapes of the nanoparticles for a sample deposited onto a surface of HOPG are shown in the topography frame (5 x 5 μm^2) in Figure 5.1A. The average diameter of the nanoparticles measured 15.1 ± 1.7 nm, derived from 100 cursor profiles. The simultaneously acquired images of surface potential and capacitance indicate that the nanoparticles are composed of a different material than the background HOPG (Figures 5.1C and 5.1D).

In the setup of the instrument, the compensating DC bias is fed from the tip to the grounded sample. A negative contact potential difference in this case, means that the work function of the nanoparticles on the HOPG sample is greater than the work function of the probe. While not of the expected magnitude, the darker contrast of the nanoparticles relative to the HOPG is expected since the experimental values for the work function of bulk gold and bulk HOPG are 5.1 eV and 4.6 eV, respectively.[36, 90] The expected value for the contact potential difference between the HOPG background and the gold nanoparticles is ~500 meV based upon [$\phi_{Au(111),lit.}$-$\phi_{HOPG,lit.}$ = $\Delta\phi_{Au(111)\text{-}HOPG}$]. The contact potential difference is directly related to the difference in work function between the gold nanoparticles and HOPG ($\Delta CPD_{Au\text{-}HOPG} = \Delta\phi_{Au\text{-}HOPG}/e$). The measured contact potential difference in the surface potential image of 6.9 ± 1.5 meV (n = 50) is

much lower than the expected value of 500 meV and can be likely be attributed to the imaging conditions under an ambient, humid environment.[19]

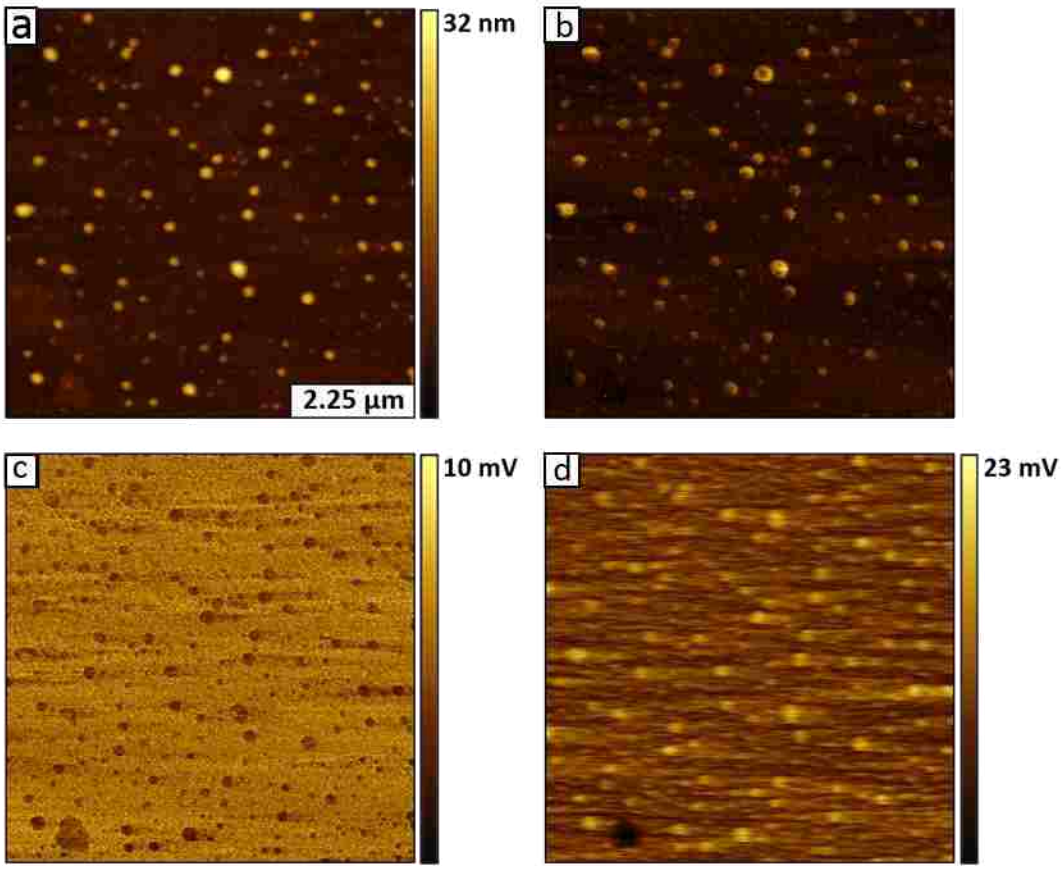

Figure 5.1. Gold nanoparticles dispersed on a HOPG substrate imaged with AM-KPFM. (a) Topography and (b) phase images obtained from the first lock-in amplifier. A three-dimensional map of the (c) surface potential and (d) capacitance.

A water layer, adsorbates, and other types of contamination may generate contact potential difference values that are lower than expected. Gold nanoparticles are a poor choice for a work function reference. The asperity noted in the lower left corner of the images has a greater work function than HOPG as evident from the darker contrast of the object relative to the HOPG background.

Gold nanoparticles with an average size of 15 nm were specifically chosen for studies because they were fairly close in size relative to the cobalt nanoparticles that were synthesized. Additionally, nanoparticles with a diameter of less than 20 nm can show effects of tip convolution where the tip will not fully resolve the size and morphology of the nanoparticles.

There is a noticeable amount of aggregation of the nanoparticles in some areas of the images as the cobalt nanoparticles can be difficult to isolate, as visualized in Figure 5.2a. There are four nanoparticles in the topography image that are prominent and of the size range 35-50 nm. The contact potential difference between the cobalt nanoparticles and the HOPG substrate measured 28.6 ± 6.0 meV as determined for the surface potential image.

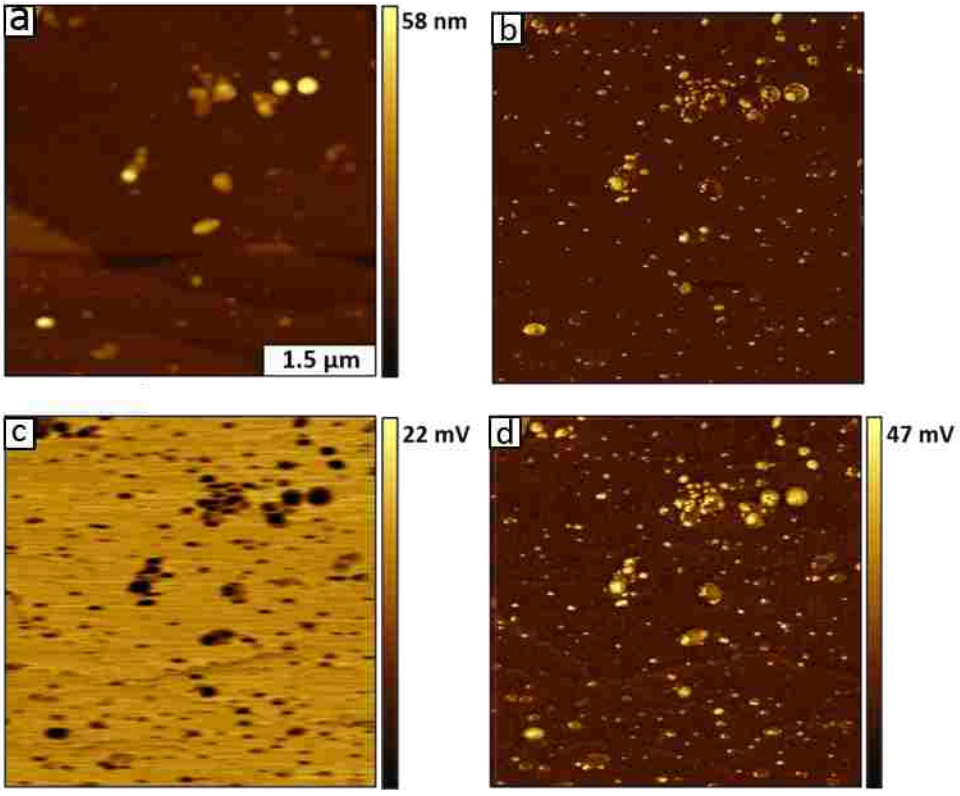

Figure 5.2. Sample of cobalt nanoparticles prepared on HOPG.(a) Topography frame viewed for an AM-KPFM image (5 x 5 μm^2); (b) phase and (c) simultaneously acquired contact potential difference and (d) surface capacitance images disclose the electrostatic properties of the sample.

As was the case with the gold nanoparticles, the cobalt nanoparticles were determined to have a higher work function than the HOPG, as would be expected. However, the magnitude of the experimental contact potential difference between the cobalt nanoparticles and HOPG was shown to be greater than the experimentally derived contact potential difference between the gold nanoparticles and the HOPG substrate. Based upon the theoretical assumption, the difference in work function between bulk cobalt and HOPG is ~400 meV [$\phi_{Co\ lit.}$-$\phi_{HOPG,lit.}$ = $\Delta\phi_{Co\text{-}HOPG}$]. The fact that the experimentally derived magnitude of the contact potential difference between cobalt nanoparticles and HOPG is greater than the contact potential difference between the gold nanoparticles and HOPG shows the shortcomings of Kelvin probe imaging in ambient conditions.

Surface potential measurements of both cobalt nanoparticle and gold nanoparticles on HOPG were compared side-by-side in Figure 5.3. The top panel presents the topography and surface potential images of the gold nanoparticles on HOPG. Four gold nanoparticles with diameters near 15 nm are clearly visible in the image along with smaller gold nanoparticles scattered in the background. The accompanying surface potential image shows less contrast between structures in the image, however, a band of high contrast is evident. The contact potential difference between the gold nanoparticle and the HOPG is roughly 10 meV.

Two of the larger cobalt nanoparticles that were present in the sample were isolated and analyzed using the amplitude modulation mode of the Kelvin probe force microscope.

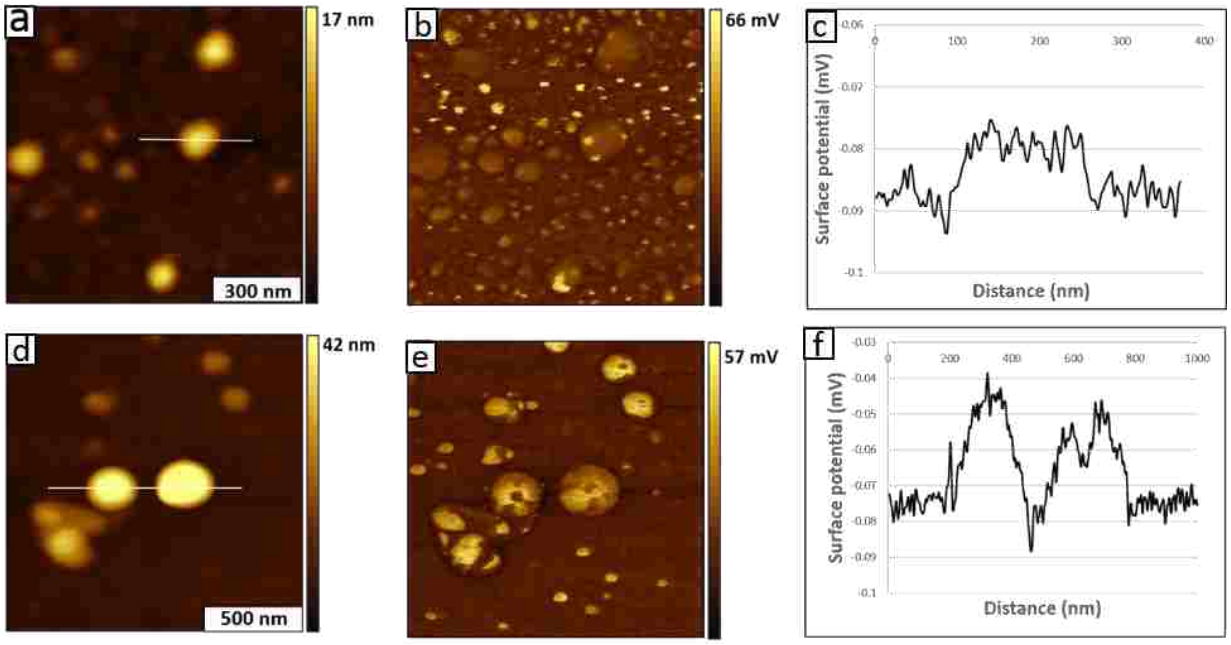

Figure 5.3. Comparison of the experimentally measured contact potential difference between gold and cobalt nanoparticles prepared on HOPG. (a) Topography and (b) simultaneously acquired surface potential images of gold nanoparticles. (c) Cursor profile detailing surface potential variance between gold and HOPG. (d) Topography and (e) surface potential images of cobalt nanoparticles. (f) Surface potential variance between gold and HOPG determined with a cursor profile.

The experimental contact potential difference between the cobalt nanoparticles and the HOPG, as measured with the cursor profile, is ~40 meV. Though smaller in size when viewed in the topography image, other cobalt nanoparticles produced similar measured potentials.

Juxtaposition of the measured contact potential differences of gold nanoparticles on HOPG and cobalt nanoparticles on HOPG reveals that the cobalt nanoparticles display a higher contact potential difference. This is contrary to the expectation based on theory that, based upon a greater difference in work function, the potential between gold nanoparticles and the HOPG substrate should be greater than the potential between cobalt nanoparticles and HOPG substrate.

The conflict between the theoretical and experimental value obtained for the contact potential difference can possibly be explained by numerous potential sources of error. Temporal variances in work function measurements have shown that the time between sample preparation and imaging is crucial in producing the sharpest contrast possible as adsorbates and humidity greatly impact the experimental values.[19] The samples used in this experiment were prepared and then subsequently placed in a vacuum oven at reduced pressure and 50 C. Samples were immediately imaged after removal from the drying oven as to minimize the adsorbate build up on the surface.

The data resulting from a side-by-side comparison of the contact potential difference of the two samples of nanoparticles was inconclusive based upon differences in theoretical and experimental values. However, further elucidation into determining how the contact potential difference varies between the gold nanoparticle-HOPG sample and cobalt nanoparticle-HOPG sample is needed to minimize sample contamination between imaging of the samples. Cobalt nanoparticles and gold nanoparticles were deposited onto a common HOPG substrate and imaged with AM-KPFM as displayed in Figure 5.4. The image is representative of the numerous other areas of the sample that were imaged and shows a relatively disperse sample of nanoparticles on HOPG.

Nanoparticles varying in size between a few nanometers in diameter up to 40 nm in diameter are present as viewed in the topography image of Figure 5.4a. Along with the phase image, the surface potential and capacitance seen in Figure 5.4c and 5.4d, respectively, exhibit streaking that is only present in the bottom half of the image which can be attributed to non-optimized imaging parameters.

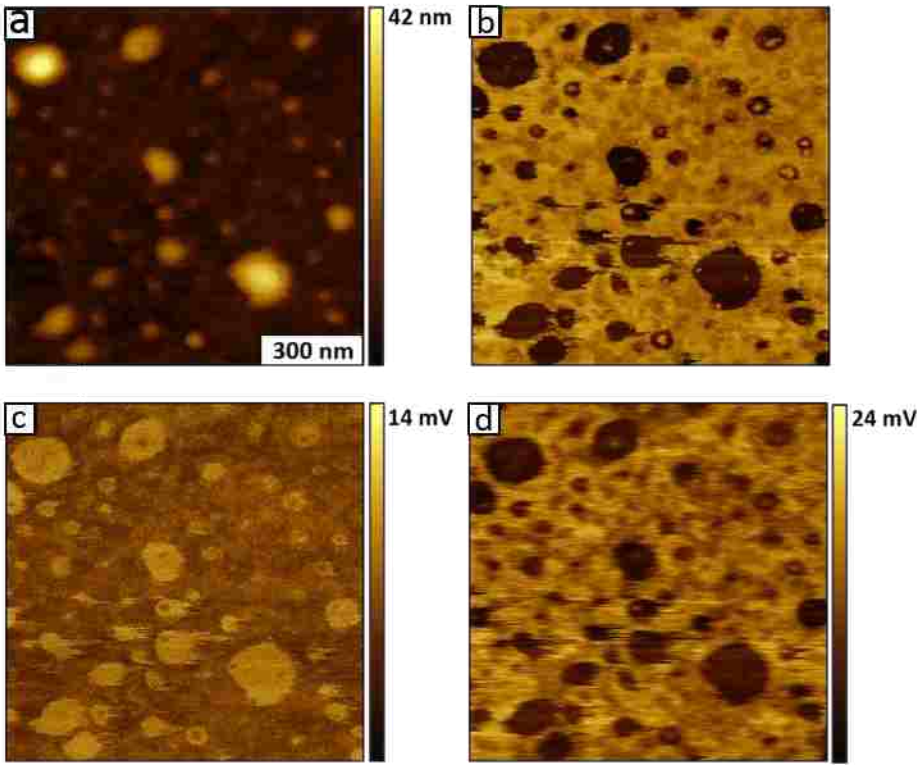

Figure 5.4. Co-deposited sample of cobalt nanoparticles and gold nanoparticles on HOPG. (a) Topography and (b) simultaneously acquired phase image acquired while imaging with AM-KPFM. (c) Contact potential difference and (d) capacitance frames furnish details of the electrostatic differences in the composition of the sample.

Surface potential and capacitance values seem unaffected by the streaking as contrast in the top of each of the images is similar to the area where streaking is observed. When comparing nanoparticles of similar sizes, there is seems to be no variance in surface potential or capacitance between the different materials. As this is also prevalent in similar images taken of the same sample, it is concluded that there is not a great enough difference in the work function of the two metals to be resolved using the current Kelvin Probe Force Microscope set-up in ambient conditions. Results that display a homogeneity in particle size and morphology but have varying contact potential differences were not observed.

5.4 Conclusions

Differentiating between dissimilar nanoparticles based solely upon the inherent differences in their work functions using KPFM was the goal of this project. There was a difference between the experimental and theoretical measurements for the contact potential difference between gold and the platinum coated AFM probe that can likely be attributed to imaging under ambient conditions. Similarly, cobalt nanoparticles of similar size also displayed a relatively large difference between the measured and theoretical contact potential difference. There was a negligible difference in contrast between the gold and cobalt nanoparticles when they were imaged together on the same sample. With dissimilar theoretical contact potential differences, differentiating between the gold and cobalt nanoparticles should be attainable with this imaging technique. As such, under ambient conditions, the limit of resolution for the instrument is likely not low enough to discriminate between the dissimilar nanoparticles. Future work dealing with nanoparticles displaying a greater difference in contact potential difference will be attempted.

CHAPTER 6. CONCLUSIONS AND FUTURE DIRECTIONS

6.1 Conclusions

Nanoparticles have become important for the development of technology because the inherent physical and chemical properties can be tailored to specific applications. In this dissertation experiments were designed and conducted to detect, elucidate, and further understand the properties of nanoparticles using advanced measurement modes of scanning probe microscopy (SPM).

Since the invention of the atomic force microscope (AFM) nearly 30 years ago, nanoscale properties have been known to be rather troublesome to accurately and precisely measure. The three methods described in this dissertation, Force Modulation Microscopy (FMM), Electrostatic Force Microscopy (EFM), and Kelvin Probe Force Microscopy (KPFM), were applied for experiments to produce high resolution images of nanoparticles. In addition to constructing 3-D surface profiles, images detailing nanoscopic elasticity, viscoelasticity, surface potential, and work function measurements were simultaneously acquired.

6.2 Subsurface imaging of encapsulated cobalt nanoparticles with FMM

Force modulation microscopy, an advanced mode of AFM, has previously been used to elucidate elastic and viscoelastic variances between co-polymer systems that cannot be distinguished using other modes of AFM. Polymer domains were intricately mapped based upon the response to an undulating force caused by the harmonic oscillation of the sample stage and tip. The study of polystyrene encapsulated cobalt nanoparticles in Chapter 4 of this dissertation used the force modulation technique to distinguish the relatively hard nanoparticle core from the softer polystyrene shell.

A home-built sample stage for use with force modulation microscopy enabled further study of the nanoparticles. Ferromagnetic cobalt nanoparticles were initially imaged with tapping-mode AFM to determine the size of the nanoparticles. The average particle diameter was found to be 26 ± 2 nm. Initial imaging of the particles using FMM provided corroboration that the measured particle size with FMM was consistent with tapping-mode data. When the stage was turned off half way through acquisition of an image there was no contrast in the amplitude and phase channels. However, with no change in the topography channel was detected.

Single nanoparticle resolution, along with resolution of subsurface features, was obtained with optimized parameters. Based upon the working theory of FMM, the amplitude signal increases as the tip is scanned across more rigid areas of the sample while there is a larger attenuation of signal in areas of the sample with greater deformation. The cobalt core of the nanoparticles exhibited greater signal in the amplitude channel because it is more rigid than the surrounding shell of the polystyrene coating.

A comparative study between a polystyrene encapsulated cobalt nanoparticle and a similarly sized polystyrene nanoparticle was done. A high resolution image of the polymer coated nanoparticle was compared with a similarly high resolution image of a single polystyrene nanoparticle. While exhibiting similar topographical similarities between the two nanoparticles, the differences in the amplitude and phase channels were sufficient to conclude that the cobalt cores of the polystyrene encapsulated cobalt nanoparticles were, indeed, resolved to accomplish subsurface imaging using FMM.

This study contributes to the overall goal of this dissertation by providing a slightly new way to use force modulation microscopy; as an additional new tool for disambiguating nanoscopic materials based on criteria not related to their size.

6.3 Designed experiments for characterizing nanoparticles with the Kelvin Probe Force Microscope

An in-depth fundamental research question is posed: can nanoparticles with dissimilar work functions be recognized and sorted based only on the differences in the measured surface potential of a sample? This question was investigated using the Kelvin Probe Force Microscope to analyze a sample of gold nanoparticles that were co-deposited onto HOPG with similarly sized cobalt nanoparticles.

Cobalt nanoparticles and gold nanoparticle were analyzed separately to obtain baseline readings of how the individual surface potentials measured relative to the HOPG samples surface. With a compensating DC bias being applied from the tip to the sample, the expected contact potential difference was much lower, with values of 500 meV theoretical vs. 22 meV experimental, than what was expected. While there was a dissimilarity in the size of nanoparticles, much of the measurement error can be ascribed to non-optimum imaging conditions. Studies in UHV and cryogenic experimental conditions would likely lead to more accurate results.

The experimentally derived contact potential difference between the tip and gold nanoparticles revealed similar results. The measured contact potential difference was different by nearly two orders of magnitude. However, as expected based upon theoretical predictions,

the gold nanoparticles displayed a greater work function value than the background measured for HOPG.

Based upon theoretical predictions, the contact potential difference between gold nanoparticles and HOPG should be greater in magnitude than the contact potential difference between cobalt nanoparticles and HOPG. However, experimental results differ from the theoretical assumption and leads to possibly erroneous results. Gold and cobalt nanoparticles were co-deposited onto the HOPG substrate and imaged simultaneously to ensure identical imaging conditions. While not using optimum imaging conditions, the inherent difference in surface potential between the nanoparticles should be revealed when imaged together.

Multiple area of the sample surface were investigated with little variance between the data collected. This leads to the assumption that there is not enough difference in measured surface potential between the two different types of nanoparticles to register a great enough difference in contrast. Greater homogeneity in particle size of each material may lower the error associated with the measurements but would not likely lead to the ability to resolve the dissimilarities between the nanoparticles under the specific parameters and conditions used for KPFM studies.

6.4 Considerations for future research experiments

Much of the research into nanomaterials relies heavily upon experimental methods that analyze the sample as a whole i.e. X-ray diffraction analysis of nanoparticles only provides an average size and not individual nanoparticles. Force modulation microscopy and Kelvin Probe Force Microscopy with individual nanoparticles reveals subtle details, and even slight incongruities, found in their inherent physical and chemical properties.

In Chapter 3 the physical properties of core-shell nanoparticles were selected to reveal differences in elastic and viscoelastic properties between a softer polystyrene shell and a harder cobalt nanoparticle core. Subsurface imaging of the metal cores of encapsulated nanoparticles was accomplished with optimized conditions. Further progress in the use of FMM on nanomaterials may lead to studies that can quantitatively compare the Young's modulus of similar core-shell nanoparticle systems.

Further investigations into the use of Kelvin Probe Force Microscopy for nanomaterials research offer exciting insight into the properties of nanoparticles that are generally only understood based on theoretical models. More specifically, another attempt at distinguishing between electronically dissimilar nanoparticles can be made with designed experiments. Nanoparticles will be specifically chosen based on how different the individual work functions are from each other. A greater difference in the work function between dissimilar nanoparticles will ideally draw greater gradients in contrast than what was experimentally revealed with the cobalt nanoparticle co-deposited with gold nanoparticles. For instance, I suggest the use of non-metallic nanoparticles to compare in a side-by-side fashion with non-metallic nanoparticles. Polymer or silica based nanoparticles may provide the similarity in particle size while also delivering a much greater change in contact potential difference than detected for two metal nanoparticles. If improved imaging conditions are attainable, I suggest replicating the experiment to investigate if dissimilar metals can be identified based solely on the inherent work functions.

REFERENCES

1. Binnig, G.; Quate, C. F.; Gerber, C. Atomic Force Microscope. *Phys. Rev. Lett.* **1986,** *56*, 930-933.

2. Hoffmann, P. M.; Oral, A.; Grimble, R. A.; Özgür özer, H.; Jeffery, S.; Pethica, J. B. Direct measurement of interatomic force gradients using an ultra-low-amplitude atomic force microscope. *Proc. R. Soc. London,* **2001,** *457*, 1161-1174.

3. Sugimoto, Y.; Pou, P.; Abe, M.; Jelinek, P.; Perez, R.; Morita, S.; Custance, O. Chemical identification of individual surface atoms by atomic force microscopy. *Nature* **2007,** *446*, 64-67.

4. Magonov, S. N.; Reneker, D. H. Characterization of polymer surfaces with atomic force microscopy. *Ann. Rev. Mater. Sci.* **1997,** *27*, 175-222.
5. Tu, R.; Zhang, L.; Nishi, Y.; Dai, H. Measuring the Capacitance of Individual Semiconductor Nanowires for Carrier Mobility Assessment. *Nano Letters* **2007,** *7*, 1561-1565.

6. Hudlet, S.; Saint Jean, M.; Guthmann, C.; Berger, J. Evaluation of the capacitive force between an atomic force microscopy tip and a metallic surface. *Eur. Phys. J. B.* **1998,** *2*, 5-10.

7. Houzé, F.; Meyer, R.; Schneegans, O.; Boyer, L. Imaging the local electrical properties of metal surfaces by atomic force microscopy with conducting probes. *Appl. Phys. Lett.* **1996,** *69*, 1975-1977.

8. Lü, J.; Delamarche, E.; Eng, L.; Bennewitz, R.; Meyer, E.; Güntherodt, H. J. Kelvin Probe Force Microscopy on Surfaces: Investigation of the Surface Potential of Self-Assembled Monolayers on Gold. *Langmuir* **1999,** *15*, 8184-8188.

9. Coffey, D. C.; Ginger, D. S. Time-resolved electrostatic force microscopy of polymer solar cells. *Nat. Mater.* **2006,** *5*, 735-740.

10. Benson, J. D.; Bubulac, L. O.; Smith, P. J.; Jacobs, R. N.; Markunas, J. K.; Jaime-Vasquez, M.; Almeida, L. A.; Stoltz, A. J.; Wijewarnasuriya, P. S.; Brill, G.; Chen, Y.; Lee, U.; Vilela, M. F.; Peterson, J.; Johnson, S. M.; Lofgreen, D. D.; Rhiger, D.; Patten, E. A.; Goetz, P. M. Characterization of Dislocations in (112)B HgCdTe/CdTe/Si. *J. Electron. Mater.* **2010,** *39*, 1080-1086.

11. Hochwitz, T.; Henning, A. K.; Levey, C.; Daghlian, C.; Slinkman, J.; Never, J.; Kaszuba, P.; Gluck, R.; Wells, R.; Pekarik, J.; Finch, R. Imaging integrated circuit dopant profiles with the force-based scanning Kelvin probe microscope. *J. Vac. Sci. Technol., B.* **1996,** *14*, 440-446.

12. Krauss, T. D.; Brus, L. E. Electronic properties of single semiconductor nanocrystals: optical and electrostatic force microscopy measurements. *Mater. Sci. Eng. B.* **2000,** *69–70*, 289-294.

13. Gross, L.; Mohn, F.; Liljeroth, P.; Repp, J.; Giessibl, F. J.; Meyer, G. Measuring the Charge State of an Adatom with Noncontact Atomic Force Microscopy. *Science* **2009,** *324*, 1428-1431.

14. Nonnenmacher, M.; O'Boyle, M. P.; Wickramasinghe, H. K. Kelvin probe force microscopy. *Appl. Phys. Lett.* **1991,** *58*, 2921-2923.

15. Shin-ichi, K.; Masashi, I. Observation of 7×7 Reconstructed Structure on the Silicon (111) Surface using Ultrahigh Vacuum Noncontact Atomic Force Microscopy. *Jpn. J. Appl. Phys.* **1995,** *34*, L145.

16. Han, W.; Mou, J.; Sheng, J.; Yang, J.; Shao, Z. Cryo Atomic Force Microscopy: A New Approach for Biological Imaging at High Resolution. *Biochemistry* **1995,** *34*, 8215-8220.

17. Kitamura, S. i.; Iwatsuki, M. High-resolution imaging of contact potential difference with ultrahigh vacuum noncontact atomic force microscope. *Appl. Phys. Lett.* **1998,** *72*, 3154-3156.

18. Hong, J. W.; Park, S.-i.; Khim, Z. G. Measurement of hardness, surface potential, and charge distribution with dynamic contact mode electrostatic force microscope. *Rev. Sci. Instrum.* **1999,** *70*, 1735-1739.

19. Palacios-Lidón, E.; Henry, C. R.; Barth, C. Kelvin Probe Force Microscopy in Surface Chemistry: Reactivity of Pd Nanoparticles on Highly Oriented Pirolytic Graphite. *ACS Catalysis* **2014,** *4*, 1838-1844.

20. Melitz, W.; Shen, J.; Kummel, A. C.; Lee, S. Kelvin probe force microscopy and its application. *Surf. Sci. Rep.* **2011,** *66*, 1-27.

21. Kahn, A. Fermi level, work function and vacuum level. *Mater. Hor.* **2016,** *3*, 7-10.

22. Jacobs, H. O.; Leuchtmann, P.; Homan, O. J.; Stemmer, A. Resolution and contrast in Kelvin probe force microscopy. *J. Appl. Phys.* **1998,** *84*, 1168-1173.

23. Martin, Y.; Abraham, D. W.; Wickramasinghe, H. K. High-resolution capacitance measurement and potentiometry by force microscopy. *Appl. Phys. Lett.* **1988,** *52*, 1103-1105.

24. Zerweck, U.; Loppacher, C.; Otto, T.; Grafström, S.; Eng, L. M. Accuracy and resolution limits of Kelvin probe force microscopy. *Phys. Rev. B.* **2005,** *71*, 125424.

25. Jespersen, T. S.; Nygård, J. Charge Trapping in Carbon Nanotube Loops Demonstrated by Electrostatic Force Microscopy. *Nano Letters* **2005,** *5*, 1838-1841.

26. Heinz, W. F.; Hoh, J. H. Relative Surface Charge Density Mapping with the Atomic Force Microscope. *Biophys. J.* **1999,** *76*, 528-538.

27. Belaidi, S.; Girard, P.; Leveque, G. Electrostatic forces acting on the tip in atomic force microscopy: Modelization and comparison with analytic expressions. *J. Appl. Phys.* **1997,** *81*, 1023-1030.

28. Salomao, F. C.; Lanzoni, E. M.; Costa, C. A.; Deneke, C.; Barros, E. B. Determination of High-Frequency Dielectric Constant and Surface Potential of Graphene Oxide and Influence of Humidity by Kelvin Probe Force Microscopy. *Langmuir* **2015,** *31*, 11339-43.

29. Zaghloul, U.; Koutsoureli, M.; Wang, H.; Coccetti, F.; Papaioannou, G.; Pons, P.; Plana, R. Assessment of dielectric charging in electrostatically driven MEMS devices: A comparison of available characterization techniques. *Microelectron. Abil.* **2010,** *50*, 1615-1620.

30. Novikov, S. N.; Timoshenkov, S. P. Measurements of contact potential difference (work functions) of metals and semiconductors surface by the static ionized capacitor method. *Adv. Colloid Interface Sci.***2003,** *105*, 329-339.

31. Dominik, Z.; Jörg, R.; Nicola, N.; Andreas, S. Compensating electrostatic forces by single-scan Kelvin probe force microscopy. *Nanotechnology* **2007,** *18*, 225505.

32. Stark, R. W. Bistability, higher harmonics, and chaos in AFM. *Mater. Today* **2010,** *13*, 24-32.

33. Th, G.; Zimmerli, L.; Koch, S.; Such, B.; Kawai, S.; Meyer, E. Determination of effective tip geometries in Kelvin probe force microscopy on thin insulating films on metals. *Nanotechnol.* **2009,** *20*, 264016.

34. Koley, G.; Spencer, M. G.; Bhangale, H. R. Cantilever effects on the measurement of electrostatic potentials by scanning Kelvin probe microscopy. *Appl. Phys. Lett.* **2001,** *79*, 545-547.

35. Elias, G.; Glatzel, T.; Meyer, E.; Schwarzman, A.; Boag, A.; Rosenwaks, Y. The role of the cantilever in Kelvin probe force microscopy measurements. *Beilstein J. Nanotechnol.* **2011,** *2*, 252-260.

36. Glatzel, T.; Sadewasser, S.; Lux-Steiner, M. C. Amplitude or frequency modulation-detection in Kelvin probe force microscopy. *Appl. Surf. Sci.* **2003,** *210*, 84-89.

37. Rosenwaks, Y.; Shikler, R.; Glatzel, T.; Sadewasser, S. Kelvin probe force microscopy of semiconductor surface defects. *Phys. Rev. B.* **2004,** *70*, 085320.

38. Nielsen, D. A.; Popok, V. N.; Pedersen, K. Modelling and experimental verification of tip-induced polarization in Kelvin probe force microscopy measurements on dielectric surfaces. *J. Appl. Phys.* **2015,** *118*, 195301.

39. Barth, C.; Hynninen, T.; Bieletzki, M.; Henry, C. R.; Foster, A. S.; Esch, F.; Heiz, U. AFM tip characterization by Kelvin probe force microscopy. *New J. Phys.* **2010,** *12*, 093024.

40. Eliseev, E. A.; Kalinin, S. V.; Jesse, S.; Bravina, S. L.; Morozovska, A. N. Electromechanical detection in scanning probe microscopy: Tip models and materials contrast. *J. Appl. Phys.* **2007,** *102*, 014109.

41. Glatzel, T.; Lux-Steiner, M. C.; Strassburg, E.; Boag, A.; Rosenwaks, Y., Principles of Kelvin Probe Force Microscopy. In *Scanning Probe Microscopy: Elec. Electromech. Phen. Nano.*, Kalinin, S.; Gruverman, A., Eds. Springer New York: New York, NY, 2007; pp 113-131.

42. Ma, Z.-M.; Mu, J.-L.; Tang, J.; Xue, H.; Zhang, H.; Xue, C.-Y.; Liu, J.; Li, Y.-J. Potential sensitivities in frequency modulation and heterodyne amplitude modulation Kelvin probe force microscopes. *Nano. Res. Lett.* **2013,** *8*, 532-532.

43. Sadewasser, S.; Jelinek, P.; Fang, C.-K.; Custance, O.; Yamada, Y.; Sugimoto, Y.; Abe, M.; Morita, S. New Insights on Atomic-Resolution Frequency-Modulation Kelvin-Probe Force-Microscopy Imaging of Semiconductors. *Phys. Rev. Lett.* **2009,** *103*, 266103.

44. Giessibl, F. J. Advances in atomic force microscopy. *Rev. Mod. Phys.* **2003,** *75*, 949-983.

45. O'Boyle, M. P.; Hwang, T. T.; Wickramasinghe, H. K. Atomic force microscopy of work functions on the nanometer scale. *Appl. Phys. Lett.* **1999,** *74*, 2641-2642.

46. Sommerhalter, C.; Glatzel, T.; Matthes, T. W.; Jäger-Waldau, A.; Lux-Steiner, M. C. Kelvin probe force microscopy in ultra high vacuum using amplitude modulation detection of the electrostatic forces. *Appl. Surf. Sci.* **2000,** *157*, 263-268.

47. Jacobs, H. O.; Knapp, H. F.; Stemmer, A. Practical aspects of Kelvin probe force microscopy. *Rev. Sci. Instrum.* **1999,** *70*, 1756-1760.

48. Parkinson, B. A.; Ren, J.; Whangbo, M. H. Relationship of STM and AFM images to the local density of states in the valence and conduction bands of rhenium selenide (ReSe2). *J. Amer. Chem. Soc.***1991,** *113*, 7833-7837.

49. Poon, C. Y.; Bhushan, B. Comparison of surface roughness measurements by stylus profiler, AFM and non-contact optical profiler. *Wear* **1995,** *190*, 76-88.

50. Mikulski, P. T.; Harrison, J. A. Packing-Density Effects on the Friction of n-Alkane Monolayers. *J. Amer. Chem. Soc.* **2001,** *123*, 6873-6881.

51. Gruverman, A.; Kolosov, O.; Hatano, J.; Takahashi, K.; Tokumoto, H. Domain structure and polarization reversal in ferroelectrics studied by atomic force microscopy. *J. Vac. Sci. Tech.***1995,** *13*, 1095-1099.

52. Martin, Y.; Wickramasinghe, H. K. Magnetic imaging by ‘‘force microscopy’’ with 1000 Å resolution. *Appl. Phys. Lett.* **1987,** *50*, 1455-1457.

53. Vesenka, J.; Manne, S.; Giberson, R.; Marsh, T.; Henderson, E. Colloidal gold particles as an incompressible atomic force microscope imaging standard for assessing the compressibility of biomolecules. *Biophys. J* **1993,** *65*, 992-7.

54. Price, W. J.; Leigh, S. A.; Hsu, S. M.; Patten, T. E.; Liu, G.-y. Measuring the Size Dependence of Young's Modulus Using Force Modulation Atomic Force Microscopy†. *J. Phys. Chem.* **2005,** *110*, 1382-1388.

55. Troyon, M.; Wang, Z.; Pastre, D.; Lei, H. N.; Hazotte, A. Force modulation microscopy for the study of stiff materials. *Nanotech.* **1997,** *8*, 163.

56. Radmacher, M.; Tillmann, R. W.; Gaub, H. E. Imaging viscoelasticity by force modulation with the atomic force microscope. *Biophys. J.* **1993,** *64*, 735-742.

57. Maivald, P.; Butt, H. J.; Gould, S. A. C.; Prater, C. B.; Drake, B.; Gurley, J. A.; Elings, V. B.; Hansma, P. K. Using force modulation to image surface elasticities with the atomic force microscope. *Nanotech.* **1991,** *2*, 103.

58. Yamamoto, S.-i.; Yamada, H. Interpretation of Direct and Indirect Force Modulation Methods Using Polymer Films. *Langmuir* **1997,** *13*, 4861-4864.

59. Force Modulation AFM of Elastomer Blends: Morphology, Fillers and Cross-linking. *Surf. Inter. Anal.* **1997,** *25*, 418.

60. Kuniko, K.; Kei, K.; Hirofumi, Y.; Kazumi, M. Submolecular resolution viscoelastic imaging of a poly(p-toluene-sulfonate) single crystal using force modulation microscopy. *Nanotech.* **2008,** *19*, 065701.

61. Jourdan, J. S.; Cruchon-Dupeyrat, S. J.; Huan, Y.; Kuo, P. K.; Liu, G. Y. Imaging Nanoscopic Elasticity of Thin Film Materials by Atomic Force Microscopy: Effects of Force Modulation Frequency and Amplitude. *Langmuir* **1999,** *15*, 6495-6504.

62. Eric, T.; Roger, L.; Bernard, N. Quantitative approach towards the measurement of polypropylene/(ethylene-propylene) copolymer blends surface elastic properties by AFM. *Nanotech.***1998,** *9*, 305.

63. Ebeling, D.; Eslami, B.; Solares, S. D. J. Visualizing the Subsurface of Soft Matter: Simultaneous Topographical Imaging, Depth Modulation, and Compositional Mapping with Triple Frequency Atomic Force Microscopy. *ACS Nano* **2013,** *7*, 10387-10396.

64. Bull, M. M.; Chung, W. J.; Anderson, S. R.; Kim, S.-j.; Shim, I.-B.; Paik, H.-j.; Pyun, J. Synthesis of ferromagnetic polymer coated nanoparticles on multi-gram scale with tunable particle size. *J. Mater. Chem.* **2010,** *20*, 6023-6025.

65. Frimpong, R. A.; Hilt, J. Z. Magnetic nanoparticles in biomedicine: synthesis, functionalization and applications. *Nanomed. (London, England)* **2010,** *5*, 1401-14.

66. Gao, J.; Gu, H.; Xu, B. Multifunctional Magnetic Nanoparticles: Design, Synthesis, and Biomedical Applications. *Acc. Chem. Res.* **2009,** *42*, 1097-1107.

67. Lu, A.-H.; Salabas, E. L.; Schüth, F. Magnetic Nanoparticles: Synthesis, Protection, Functionalization, and Application. *Ang. Chem. Int. Ed.* **2007,** *46*, 1222-1244.

68. Garno, J. C.; Amro, N. A.; Wadu-Mesthrige, K.; Liu, G.-Y. Production of Periodic Arrays of Protein Nanostructures Using Particle Lithography. *Langmuir* **2002,** *18*, 8186-8192.

69. Mullen, T. J.; Zhang, M.; Feng, W.; El-khouri, R. J.; Sun, L.-D.; Yan, C.-H.; Patten, T. E.; Liu, G.-y. Fabrication and Characterization of Rare-Earth-Doped Nanostructures on Surfaces. *ACS Nano* **2011,** *5*, 6539-6545.

70. Rugar, D.; Mamin, H. J.; Guethner, P.; Lambert, S. E.; Stern, J. E.; McFadyen, I.; Yogi, T. Magnetic force microscopy: General principles and application to longitudinal recording media. *J. Appl. Phys.* **1990,** *68*, 1169-1183.

71. Hartmann, U. Magnetic force mircoscopy. *Ann. Rev. Mater. Sci.* **1999,** *29*, 53-87.

72. Daniels, S. L.; Ngunjiri, J. N.; Garno, J. C. Investigation of the magnetic properties of ferritin by AFM imaging with magnetic sample modulation. *Anal. Bioanal. Chem.* **2009,** *394*, 215-223.

73. Marshall, G. W., Jr.; Balooch, M.; Gallagher, R. R.; Gansky, S. A.; Marshall, S. J. Mechanical properties of the dentinoenamel junction: AFM studies of nanohardness, elastic modulus, and fracture. *J. Biomed. Mater. Sci.* **2001,** *54*, 87-95.

74. Hoffmann, S.; Östlund, F.; Michler, J.; Fan, H. J.; Zacharias, M.; Christiansen, S. H.; Ballif, C. Fracture strength and Young's modulus of ZnO nanowires. *Nanotech.* **2007,** *18*, 205503.

75. Wong, E. W.; Sheehan, P. E.; Lieber, C. M. Nanobeam Mechanics: Elasticity, Strength, and Toughness of Nanorods and Nanotubes. *Science* **1997,** *277*, 1971-1975.

76. Vinckier, A.; Semenza, G. Measuring elasticity of biological materials by atomic force microscopy. *FEBS Letters* **1998,** *430*, 12-16.

77. Rief, M.; Oesterhelt, F.; Heymann, B.; Gaub, H. E. Single Molecule Force Spectroscopy on Polysaccharides by Atomic Force Microscopy. *Science* **1997,** *275*, 1295-1297.

78. Puchner, E. M.; Gaub, H. E. Force and function: probing proteins with AFM-based force spectroscopy. *Curr. Opin. Struct. Biol.* **2009,** *19*, 605-614.

79. Kim, B.-H.; Palermo, N. Y.; Lovas, S.; Zaikova, T.; Keana, J.; Lyubchenko, Y. Single molecule AFM force spectroscopy study of Aβ-40 interactions. *Biochemistry* **2011,** *50*, 5154-5162.

80. Butt, H.-J. Electrostatic interaction in atomic force microscopy. *Biophys. J.* **1991,** *60*, 777-785.

81. Weaver, J. M. R.; Abraham, D. W. High resolution atomic force microscopy potentiometry. *J. Vac. Sci. Tech. B* **1991,** *9*, 1559-1561.

82. Sugimura, H.; Ishida, Y.; Hayashi, K.; Takai, O.; Nakagiri, N. Potential shielding by the surface water layer in Kelvin probe force microscopy. *Appl. Phys. Lett.* **2002,** *80*, 1459-1461.

83. Guillaumin, V.; Schmutz, P.; Frankel, G. S. Characterization of Corrosion Interfaces by the Scanning Kelvin Probe Force Microscopy Technique. *J. Electrochem. Soc.* **2001,** *148*, B163-B173.

84. Simon, M.; Jun, Y. Influence of Surface Adsorption on Work Function Measurements on Gold-Platinum Interface Using Scanning Kelvin Probe Microscopy. *J. Phys.* **2012,** *371*, 012030.

85. Hückstädt, C.; Schmidt, S.; Hüfner, S.; Forster, F.; Reinert, F.; Springborg, M. Work function studies of rare-gas/noble metal adsorption systems using a Kelvin probe. *Phys. Rev. B.* **2006,** *73*, 075409.

86. Schmidt, H.; Habicht, S.; Feste, S.; Müller, A.-D.; Schmidt, O. G. Kelvin probe force microscopy for characterizing doped semiconductors for future sensor applications in nano- and biotechnology. *Appl. Surf. Sci.* **2013,** *281*, 24-29.

87. Baumgart, C.; Helm, M.; Schmidt, H. Quantitative dopant profiling in semiconductors: A Kelvin probe force microscopy model. *Phys. Rev. B* **2009,** *80*, 085305.

88. Henning, A. K.; Hochwitz, T.; Slinkman, J.; Never, J.; Hoffmann, S.; Kaszuba, P.; Daghlian, C. Two-dimensional surface dopant profiling in silicon using scanning Kelvin probe microscopy. *J. Appl. Phys.* **1995,** *77*, 1888-1896.

89. Kittel, T.; Roduner, E. Charge Polarization at Catalytic Metal–Support Junctions. Part B: Theoretical Modeling of Kelvin Probe Force Microscopy. *J. Phys. Chem. C* **2016,** *120,* 8917-8926.

90. Sachtler, W. M. H.; Dorgelo, G. J. H.; Holscher, A. A. The work function of gold. *Surf. Sci.* **1966,** *5*, 221-229.

APPENDIX A: INSTRUMENT OPERATION PARAMETERS FOR ELECTROSTATIC FORCE MICROSCOPY

The electrostatic force microscope is used to qualitatively examine changes in the electrostatic field of samples. Differences in electrostatic fields of local domains are measured and analyzed by applying a bias voltage to the sample.

An Agilent MACIII controller is required in EFM Mode to provide the drive signals. Lock-in 1 is used to mechanically drive the cantilever. The amplitude of the cantilever deflection is the input for Lock-in 1 for topographic profiles of the sample. The desired imaging frequency is dependent upon the mechanical resonance frequency of the cantilever, and values were typically around 75 kHz. Lock-in 2 was used to provide an AC bias and operated at a different frequency, ω_{AC}, with the deflection channel as the input.

The initial setup for EFM operation requires an AC nose cone assembly such as the one used in tapping-mode AFM. Conductive tips with a resonance frequency typically between 50-100 kHz were used for EFM. Silicon probes with a Pt/Ir coating provided optimal operation of EFM mode, however, other types of conductive probes may be substituted.

1. For initial setup of the instrument:

    a) Insert the AC nose assembly into the scanner.

    b) Insert an EFM compatible probe into the nose cone assembly.

    c) Place the scanner into the microscope base and secure.

    d) Align the laser on the cantilever.

    e) Insert and align the photodetector.

2. Prepare the sample and place it on the sample plate. To ensure accurate data, the sample *must* be electrically isolated from the sample plate, otherwise the circuit will be shorted.

3. Attach a conductor from the working electrode to the sample. Ensure a good connection is made between the electrode contact and the sample.

4. Plug the 3-pin EC connector of the EC/MAC cable into the 3-pin receptor located on the sample plate. Plug the other end of the cable into the EC/MAC receptor on the microscope.

5. Close the isolation chamber containing the AFM scanner and open the Agilent 5500 imaging software.

6. In the menu option, choose **Mode > EFM or KPFM** as shown in Figure A1.

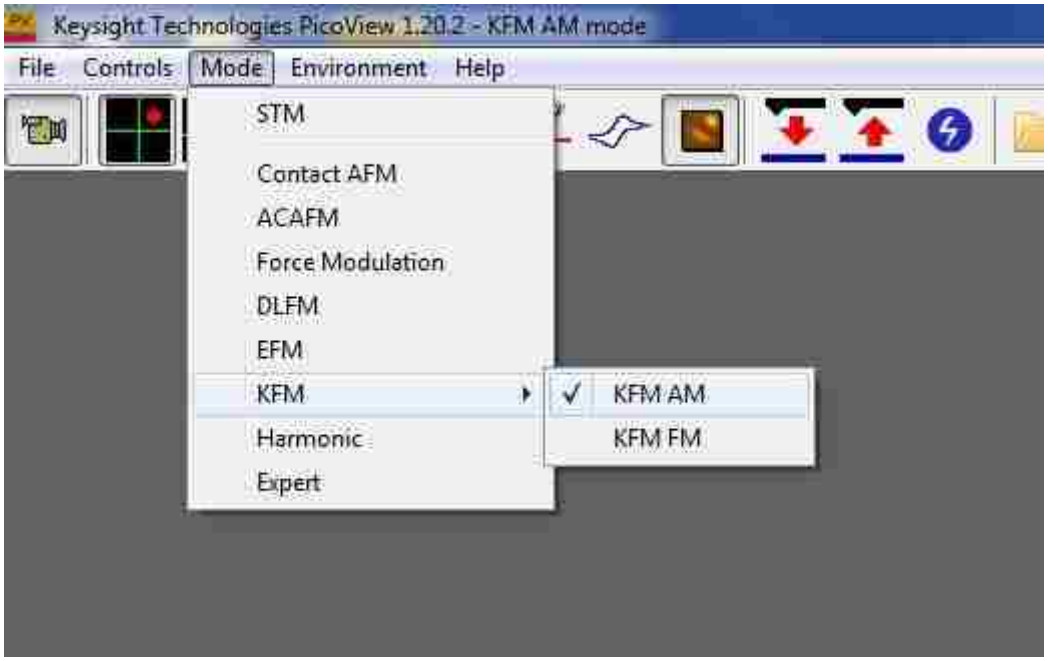

Figure A1. Software set-up for EFM mode.

7. Next, select **Controls > Advanced > AC Mode**. The EFM controls window will open.

8. The AC signal driving the mechanical cantilever oscillation is to be set up in Lock-in 1 as found in the **Main** tab (Figure A2).

a) In this window, set the **Drive %** to 10 %

b) Set the Gain to x1

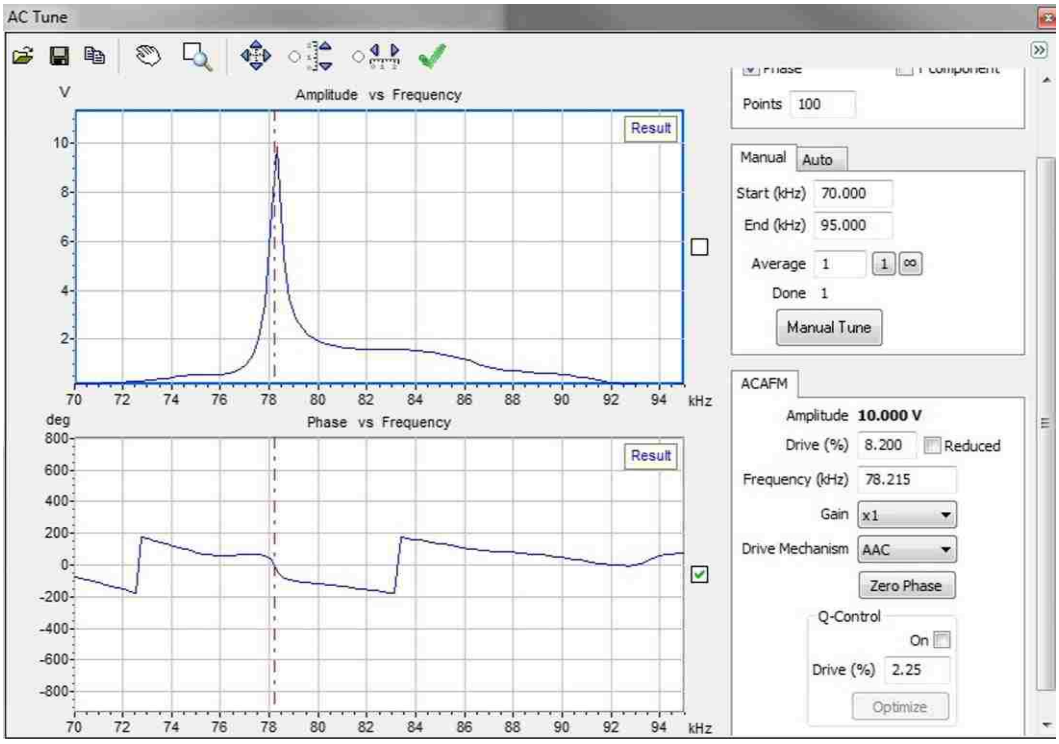

Figure A2. Software settings for driving cantilever oscillation.

9. Open the AC Mode Tune window. **Controls > AC Mode Tune**.

10. For an optimal topography channel, set the drive signal to roughly 85% of the resonance frequency of the cantilever on the lower frequency side of the peak.

a) The AC Mode Tune window will enable the user to enter **Start** and **End** values for the width of frequencies that are to be scanned. Choose between ~20-120 kHz.

b) Set the **Peak Amplitude** to **2.5** volts. Note that this is a lower peak amplitude than one that is typically used for tapping-mode (~10 volts)

c) The frequency sweep can be done using either the **Auto Tune** of **Manual Tune** option. **Auto Tune** will determine and isolate the desired resonance frequency to be used whereas manual tune gives the user a control over the exact imaging frequency to use. Generally the user will want to choose an offset of the peak amplitude by about -0.100 kHz.

11. Manually bring the tip close to the sample:

a) Bring the cantilever into focus in the video window.

b) Manually approach the tip to the sample by pressing the **Close** switch on the HEB.

12. Initiate approach with the software:

a) Locate the **Scan and Motor** window and click the **Motor** tab.

b) Set the **Stop at (%)** to 90-95%. This specifies the percentage of total oscillation the will be attenuated upon “contact” with the sample.

c) Click the **Approach** button in the PicoView toolbar. The tip and sample will converge until the tapping amplitude is dampened to the **Stop at** percentage.

13. Operation of tapping-mode AFM is now set up. Application of the AC bias is the next step.

14. The **EFM** tab is used to adjust and optimize the AC bias applied to the sample. Lock-in 2 is set up using the MAC III controller which applies the AC bias. Once activated, use the AC Tune

window to verify that the ω_{AC} signal is at a frequency that does increase unwanted tip response.

a) The **Servo** window displays the **setpoint** value. Adjust the **Setpoint** to 10 V as this will increase the tip-sample distance.

b) In the **EFM** tab, adjust the **Drive %** to 10 %. This is an important parameter as a higher value will improve contrast in the images, however, if adjusted too high, will add unwanted noise.

c) Another important parameter of note is the AC bias frequency. Set this to a frequency that is smaller than, and not an even factor of, the Lock-in 1 signal. This will cause crosstalk between the topography and electrostatic imaging modes.

d) Next, adjust the **Gain** to improve signal-to-noise ratio. Again, there is an upper bound of what the Gain can be adjusted to.

e) The **EFM Tune** check box can now be selected.

f) Perform a frequency sweep in the **AC mode tune** window, similar to the tuning of the Lock-in 1. Set **Start** and **End** frequencies around the set AC bias frequency and perform a frequency sweep.

g) Select the **Manual Tune** button. Adjust frequency in the **EFM** tab to one of the peak frequencies.

i) Return the **Setpoint** to its original value in the **Servo** window.

15. Select the **EFM Tune** box in the **EFM** tab.

16. Zeroing of the phase at the current frequency will make interpretation of the phase change easier. Click the **Zero Phase** button then select **Optimize Phase** in the **EFM** tab. **Optimize Phase** will maximize the X-component of the phase signal.
17. Set the initial **I Gain** and **P Gain** to 5% each as found in the **Servo** window. EFM Mode set up is now complete and imaging can be started. A scan speed around 1 ln/s at a resolution of either 256 or 512 is optimal.
18. Monitor and adjust the **Gain**, **Resolution**, and **Scan Speed** to optimize the imaging parameters until all frames are clearly resolved.
19. If all image panels fail to resolve, retract the tip from the surface and re-engage. The phase will need to be optimized again as will the **Scan Speed**, **Gain**, and **Resolution**.

APPENDIX B. SET-UP FOR KELVIN PROBE FORCE MICROSCOPY

The Kelvin Force Probe Microscopy mode of AFM is designed for quantitative electrostatic mapping of the surface potential. Sample preparation needs to be carefully performed as surface impurities will greatly affect the contrast and measured surface potential. Kelvin Probe Force Microscopy can be broken down into two constituent modes; Amplitude Modulation (AM-KPFM) and Frequency Modulation (FM-KPFM). Generally, AM-KPFM is regarded as the easier mode to operate for mapping the absolute potential difference, whereas, FM-KPFM is used to register the potential gradient as a function of distance. Similar to EFM, KPFM requires the use of a conductive probe, the AC nose cone assembly generally used for tapping-mode, a sample plate with electrode connection, and a MACIII controller which provides the DC bias. Since the only difference between KPFM and EFM is whether a backing potential is applied to the sample, the instrumentation set-up is similar. An additional step of setting up the DC bias is required for FM-KPFM.

To operate the Amplitude Modulation mode of KPFM, set-up up the instrument according following the instructions for EFM mode as follows.

1. Begin with the probe already approached and in contact with the sample. A backing potential needs to be applied.
2 . Select **Controls** > **Advanced** > **AC Mode** and select the **Other** tab as shown in Figure B1.

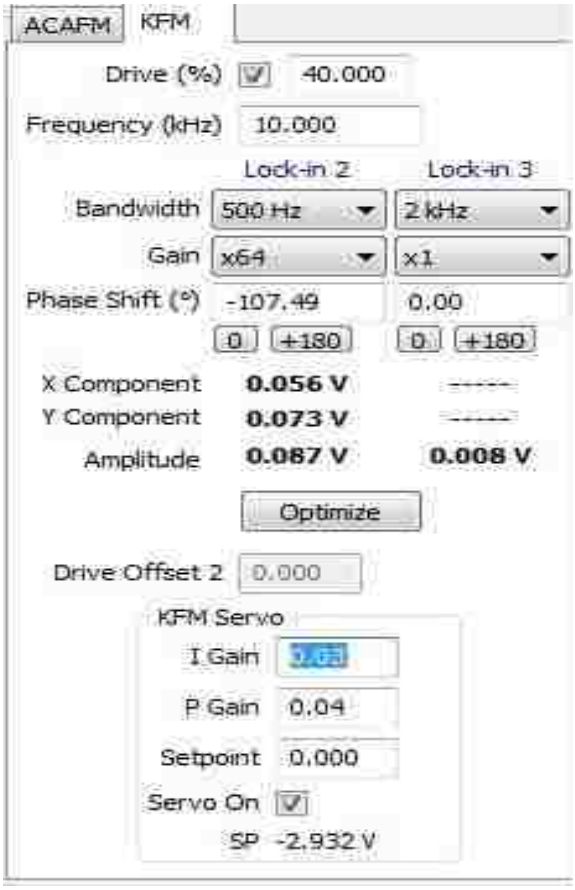

Figure B1. Software settings for KPFM.

3. Set the **I** and **P** gains initially to 1%.
4. Select the imaging channels. In the Realtime images window, choose **Topography**, **Phase**, **SP** and any other channel that should be monitored.
5. Open the spectroscopy window with **Controls** > **Spectroscopy** as shown in Figure B2.

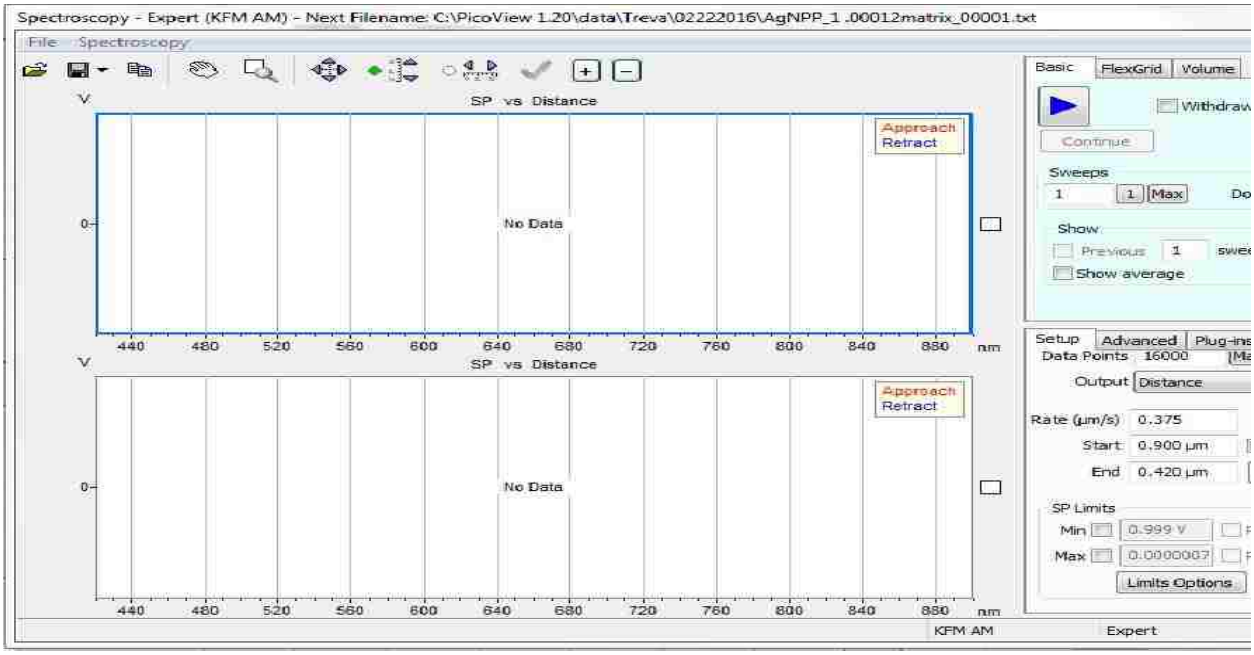

Figure B2. Spectroscopy settings for KPFM.

6. Select **Amplitude vs. Distance.**
7. Ensure that the **From Servo** box is not checked on the **Lock-in 2** tab.
8. Enter a slightly more positive value for the **End** parameter to prevent damage to the tip. Retracting the tip from the surface will lessen the likelihood of causing damage to the tip by the motion of the piezoceramic.
9. Perform a sweep detailing the SP response by clicking the blue triangle. This will begin the piezo movement.
10. The SP setpoint now needs to be optimized. Open **Advanced AC Mode Controls** and increase the Setpoint value in very small increments (0.001), as shown in Figure B3. Optimize the SP vs Distance trace by making the plot as horizontal as possible. Values of less than 0.05 are typical. End the spectroscopy step once trace and retrace are roughly horizontal.

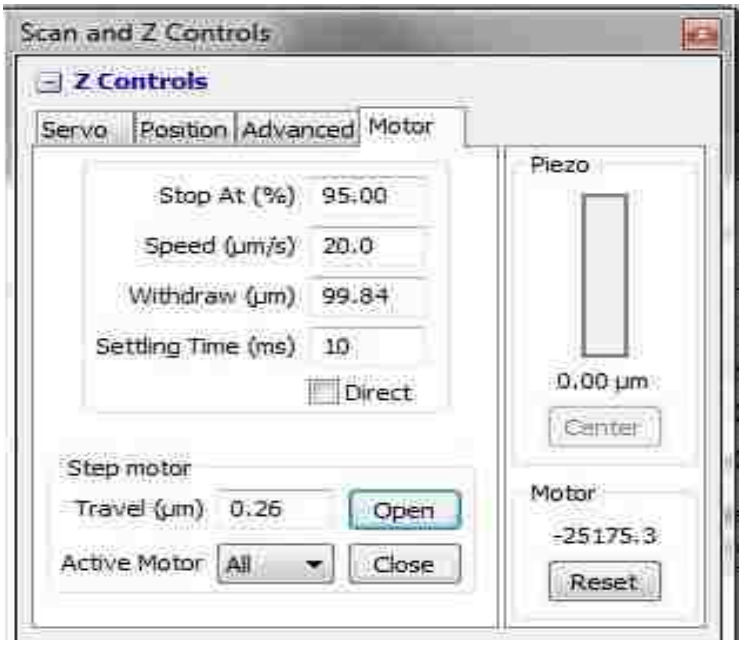

Figure B3. Controller settings for Z positioning.

11. Select the **From Servo** check box located on the **Lock-in 2** tab.

12. Begin imaging. Monitor and adjust **I** and **P** gains, **Scan Speed**, **Resolution**, **Offset**, and **AC Bias** frequency.

APPENDIX C. ADDITIONAL EXAMPLE IMAGES ACQUIRED WITH FORCE MODULATION MICROSCOPY

Additional subsurface images of polystyrene encapsulated cobalt nanoparticles were obtained with the Force Modulation mode of AFM. Two-particle lithography was used to arrange the nanoparticles into ring-shaped nanopatterns with a surface mask of a larger silica mesospheres. Removal of the silica mesospheres revealed a nanopatterned surface with relatively few defects. The nanopatterns of nanorings are evident across the entire sample.

Nanopatterned cobalt nanoparticles were imaged using Force Modulation Microscopy, revealed in the 3 µm x 3 µm topography image (Figure C1).

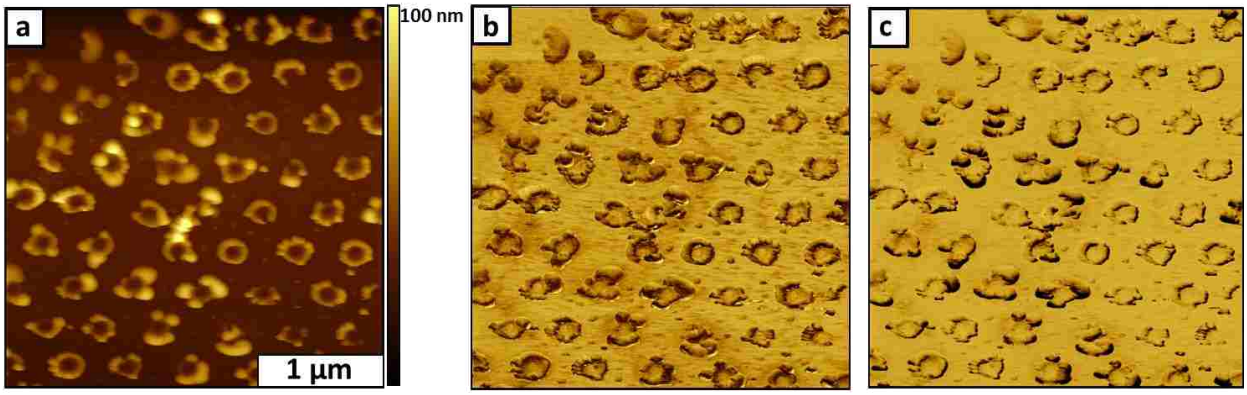

Figure C1. Polystyrene encapsulated cobalt nanoparticles formed into a high-throughput pattern of nanorings as evidenced in topography (a), amplitude (b), and phase (c) channels.

Variances in contrast evident in the amplitude frame can likely be attributed to differences in the elastic domains along with tip-sample convolution. Similar results are viewed in the phase image to clearly resolve the shapes, locations and elastic domains of the nanoring patterns.

Individual nanoparticles comprising a nanoring are resolved in the 1.5 µm x 1.5 µm images in Figure C2.

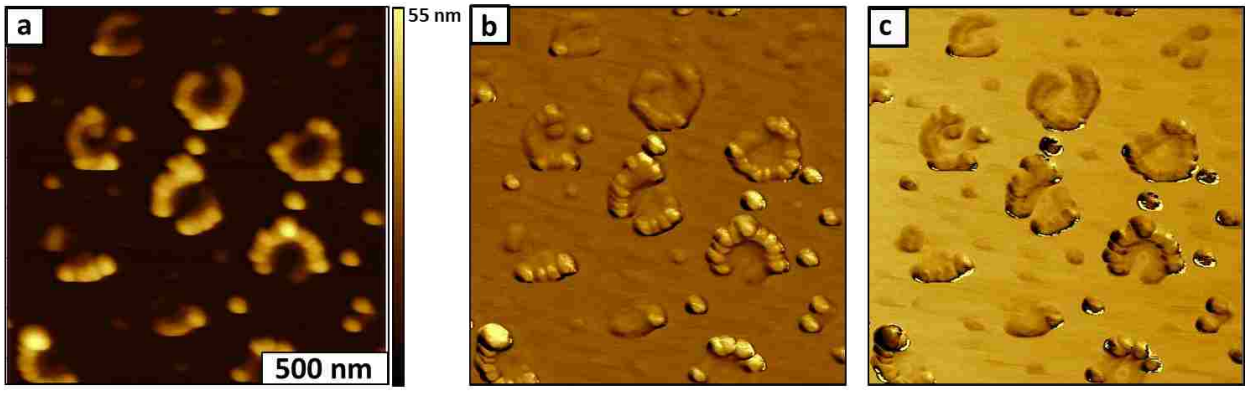

Figure C2. Individual nanoparticles comprising the shapes of the nanoring patterns. Particle sizes are evident in topography (a) whereas differences in elasticity and viscoelasticity are mapped in the amplitude (b) and phase (c) channels, respectively.

Overall, there are ~ 9 ring nanopatterns formed in a hexagonal arrangement. A full ring of nanoparticles likely consists of around 20 nanoparticles as a half-ring is formed from ten individual nanoparticles. Local elastic and viscoelastic variances between the nanoparticles and the substrate are resolved at this magnification. However, stark changes in contrast are noted in the phase image and are attributable to edge effects. Edge effects are typically caused by an abrupt change in surface topography that can alter amplitude and phase signals.

Subsurface features are apparent in the 400 nm x 400 nm^2 images viewed in Figure C3. A single nanoparticle next to a nanoring consisting of cobalt nanoparticles is evident in these images. Nanoparticles of small sizes are viewed in the topography image. The lone polystyrene encapsulated cobalt nanoparticle near the top of the image exhibits two distinct elastic and viscoelastic domains. The amplitude channel depicts a harder cobalt nanoparticle core as portrayed by the much brighter contrast at the center of the nanoparticle. The surrounding

polystyrene coating is softer and dampens the oscillation amplitude of the cantilever to a greater extent. Similarly, contrast in the phase image indicated the differences in viscoelasticity associated with the two domains of the encapsulated nanoparticles.

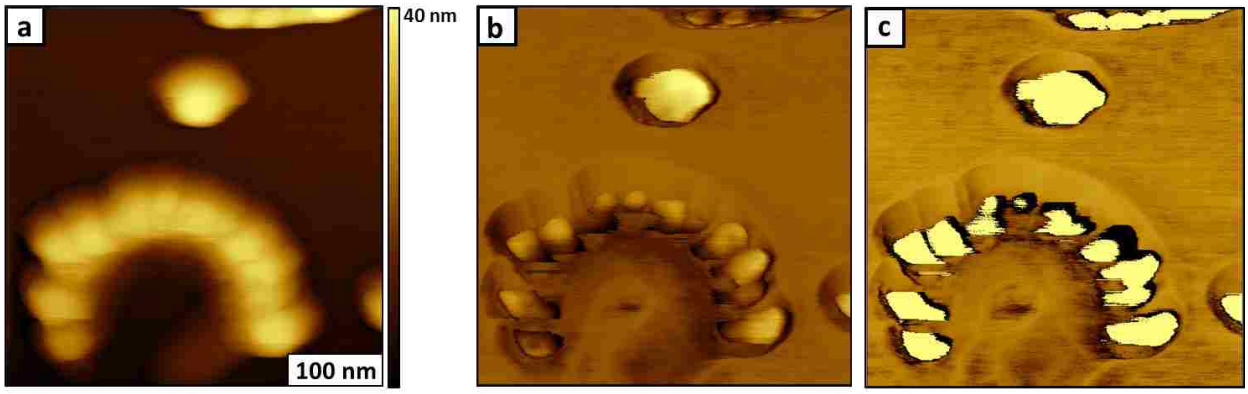

Figure C3. Subsurface imaging achieved in exquisite detail. Individual nanoparticles visualized in the topography image (a) while high quality images of variances in elasticity and viscoelasticity are detailed in (b) and (c), respectively.

Using TEM, Pyun *et* Al. reported the average size of the polymer encapsulated cobalt nanoparticles to be 25 ± 3.9 nm. Using tapping-mode AFM, the average particle size was determined to be 25 ± 3.0 nm corroborating the previous findings. Fifty individual cursor profile measurements were collected and average particle size diameter as well as the standard deviation was calculated for the sample. Determination of the thickness of the polymer coating would likely be possible with a greater amount of data. In this case, the nanoparticle diameter, as determined with TEM, has too broad of a standard deviation to calculate the thickness of the polymer. Polymer thickness can be estimated to be on the order of 0.1 – 2.0 nm. The relatively narrow range of particle sizes facilitates good packing of the nanoparticles at the base of the

mesospheres that were used as the mask for preparing samples with two-particle lithography (Figure C4).

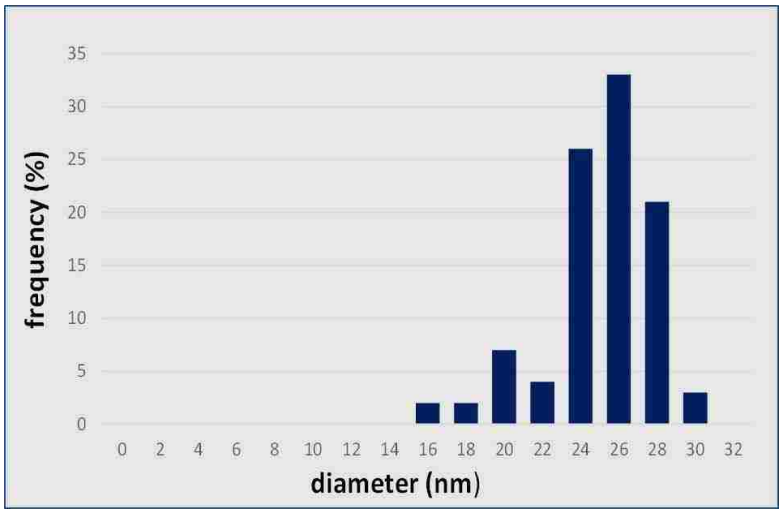

Figure C4. Size distribution of the polystyrene encapsulated cobalt nanoparticles. The average particle size was determined to be 25 ± 3.0 nm (*n* = 50).

Additional data relating to the subsurface imaging of polystyrene encapsulated cobalt nanoparticles reveal the capabilities of the FMM technique for mapping and distinguishing differences in elastic and viscoelastic domains of samples.

VITA

Steve Deese was raised and educated in Springfield, Virginia. He received his Bachelor's degree from George Mason University. During his junior and senior year at George Mason University, Steve had the unique opportunity to work at the Naval Research Laboratory in Washington, D.C. He focused on organic and polymer synthesis with Dr. Holly Ricks-Laskoski. This work led to his interests in physics and inorganic chemistry. He decided to attended graduate school at Louisiana State University with encouragement from his mentor.

For his doctoral studies, Steve studied the interesting properties of nanomaterials using the Atomic Force Microscope. His research in the field involves a mix of analytical and inorganic chemistry as he probes nanomaterials with complex modes of AFM.